JOURNAL OF GEOPHYSICAL RESEARCH OCEANS
SEP 14 2007; 112 (C9) NIL_15-NIL_33
http://dx.doi.org/10.1029/2006JC003935

An edited version of this paper was published by AGU.

A regional numerical ocean model of the circulation in the Bay of Biscay

Y. Friocourt[1,2,*] B. Levier,[1] S. Speich[1] B. Blanke[1] and S. S. Drijfhout[2]

1Laboratoire de Physique des Océans, UMR 6523 CNRS/UBO/IFREMER, Brest, France
2Royal Netherlands Meteorological Institute, De Bilt, Netherlands

*: Corresponding author : Dr. Y. Friocourt, WL j Delft Hydraulics, Environmental Hydrodynamics, Marine & Coastal Management, P.O. Box 177, 2600 MH Delft, The Netherlands (yann.friocourt@wldelft.nl)

Abstract:

The seasonal circulation along the northern Iberian Peninsula and in the Bay of Biscay is investigated by means of a regional ocean model. In particular, the modeled velocities and tracers are compared to available observations and used to hypothesize what the circulation may look like in areas where the density of observations is scarcer. Despite a few biases in the thermohaline properties of some water masses, the model is able to represent the various water masses present in the region in an acceptable way. In particular, the density and depth ranges of most water masses are in good agreement with observed ranges. Similarly, the circulation schemes compare generally well with observations, both in annual mean as for the seasonal features. The model simulates a baroclinic slope current system that extends within the upper 2000 m and is subject to a strong seasonal variability. As a result, these slope currents are seen to reverse seasonally at all depths. A numerical Lagrangian analysis indicates that water masses cannot be transported continuously within the slope currents in or out of the Bay of Biscay because of the flow reversals associated with this seasonality. Instead, this analysis highlights the numerous connections with the slope current system and the interior, in agreement with Lagrangian drifter data.

1. Introduction

The northeastern Atlantic Ocean off western Europe is a relatively sluggish part of the ocean, located southeast of the strong North Atlantic Current and north of the subtropical gyre. The mean circulation is weak compared with that in the western part of the basin, with typical velocities of a few centimeters per second. It is mainly forced by the winds and therefore markedly seasonal. In summer, the Azores high-pressure cell is located over the central Atlantic and the Greenland low-pressure cell weakens, thus resulting in southward winds along the Iberian coast; the associated offshore Ekman transport induces upwelling and southward surface circulation [*Bakun and Nelson*, 1991]. In winter, the Azores high-pressure cell is located off the northwestern African coast and the Greenland low-pressure cells intensifies, which drives northeastward winds off Iberia; however, this mean winter wind pattern is subject to high variability due to the energetic mid-latitude North Atlantic winter depressions. This wind seasonality causes large seasonal changes in the circulation; thus, this part of the ocean requires a large number of observational data in order to be described accurately.

The western Iberian upper slope region has been extensively studied and the main seasonal patterns for the upper 300 m have been described in numerous papers. *Frouin et al.* [1990] and *Haynes and Barton* [1990] introduced the Iberian Poleward Current (IPC), a poleward jet that develops in fall and winter over the Iberian and Cantabrian upper slopes and advects warm and salty waters into the Bay of Biscay (a map of the area is presented in Figure 1). The associated occurrence of warm waters along the northern coast of Spain around Christmas time is sometimes referred to as “Navidad” [*Pingree* *and Le Cann*, 1992]. Using satellite imagery, *Garcia-Soto et al.* [2002] established that the IPC is a robust feature of the winter circulation along the Iberian Peninsula, but that the eastward penetration of the jet along the Cantabrian Slope and of the associated warm water tongue in the Bay of Biscay is subject to interannual variability. The fate of the IPC in summer is still unclear: some authors report the complete disappearance of the poleward flow in the upper layers off the western Iberian Peninsula [e.g. *Haynes and Barton*, 1990], but a few observations off Portugal suggest a possible persistence of the IPC in summer, though much weakened and shifted offshore [e.g. *Peliz et al.*, 2002]. The season of upwelling-favorable winds off Iberia extends from May to October, although some brief episodes of nearshore upwelling are occasionally observed during winter in response to short-lived episodes of southward winds; however, it is not until the onset of the so-called Portuguese Trades that persistent occurrence of cold upwelled water is visible [*Haynes et al.*, 1993]. During this summer upwelling period the surface circulation is southward over the western Iberian shelf [e.g. *Castro et al.*, 1994].

The seasonal circulation off the Iberian Peninsula below 300 m as well as in the Bay of Biscay area has been much less extensively observed and described. The most notable datasets include a few moorings [e.g. *Daniault et al.*, 1994; *Pingree et al.*, 1999] or Lagrangian float data [e.g. *Van Aken*, 2002; *Colas*, 2003; *Serpette et al.*, 2006; *Le Cann et al.*, 2006]. However, all these observations also suggest occasional reversals of the slope currents. The most comprehensive dataset was obtained during the ARCANE experiment, which consisted in a large sample of Lagrangian floats and drifting buoys being released in the northeastern Atlantic [e.g. *Le Cann et al.*, 1999; *Bower et al.*, 2002]. The depth of these floats ranged from the subsurface to about 1300 m and their trajectories revealed a strong seasonality of the circulation in the Bay of Biscay [*Colas*, 2003; *Serpette et al.*, 2006; *Le Cann et al.*, 2006]. In particular, these floats evidenced the strong baroclinicity of the slope currents in the Bay of Biscay, with at least three slope currents centered respectively at about 100 to 150 m, 450 m, and 1000 m; it was also found that these slope currents are not always directed poleward and vary seasonally [*Colas*, 2003; *Serpette et al.*, 2006; *Le Cann et al.*, 2006].

Regarding numerical studies, the presence of steep continental slopes and narrow slope currents as well as the role played by mesoscale processes require a fine resolution that is very costly to implement in global ocean models or even basin-scale models of the Atlantic Ocean. A few regional studies have been carried out but they remain scarce and focused almost exclusively on the upper slope current system within the upper 400 m along the Iberian Peninsula, leaving out the Bay of Biscay area [*Stevens et al.*, 2000; *Coelho et al.*, 2002; *Peliz et al.*, 2003]. However, there is a need for numerical models of the area, both for realistic modeling and process-oriented studies, in order to overcome this knowledge gap. Indeed, the complexity of the processes that account for the observed circulation is such that their specific role and the way they interact is not yet well understood.

The present study aims to better understand the circulation in the Bay of Biscay. A regional primitive equation numerical model is used in order to present the seasonal circulation in the region in its entirety. In particular, the dynamical features obtained in this realistic simulation are compared to observations whenever possible; on account of the fair success of the comparison, the model is used to hypothesize what the circulation may look like in areas with scarcer observations. We also investigate the Lagrangian pathways of various water masses in and out of the Bay of Biscay by means of a Lagrangian numerical integration method. In this study, we only consider the main features of the circulation and its seasonal variability, and we leave out the mesoscale activity. In the following, we will sometimes refer to the "large-scale" circulation as the main features of the circulation excluding eddies. Yet, because the circulation includes narrow slope currents, the numerical model that we employ has a relatively fine resolution.

The paper is organized as follows: section 2 presents the regional ocean model. The rendering of water masses and the seasonal cycle of the model circulation are discussed in sections 3 and 4, respectively, with comparisons to observations where available. The Lagrangian pathways are presented and discussed in section 5, and we present our conclusions in section 6.

2. The Regional Model

The regional model is based on the OPA code [*Madec et al.*, 1998] with z-coordinates and a free surface [*Roullet and Madec*, 2000]. The domain covers the area 1°W–15°W and 40°N–50°N with a 6-km horizontal resolution ($\sim 1/15°$). There are 50 levels along the vertical, whose thickness varies from 10 m in the uppermost layers to 500 m near the bottom; the thickness is 60 m in the depth range of Mediterranean Water (MW, centered around 1000 m). The bathymetry was built from measurements taken during the MINT94 campaign [*Pichon*, 1997] with an original resolution of $1''$. Subgrid-scale horizontal diffusion of momentum and tracers is parameterized with biharmonic schemes along geopotential surfaces. Vertical eddy viscosity and diffusivity coefficients are computed from a 1.5 turbulent closure scheme [*Blanke and Delécluse*, 1993].

The model was spun-up from an annual climatological mass field computed from the last five years of a 16-year run of the 1/10°-resolution POP model of the North Atlantic

[*Smith et al.*, 2000], regridded onto our own model mesh. It is forced with a daily wind climatology constructed from the ECMWF ERA-15 (1979 to 1993) dataset regridded onto a 1°-grid, so that successive days are the mean of 15 distinct average daily values. the wind-stress has been averaged for each day of the year over the 15-year period. Although this method considerably reduces the day-to-day variability and total mechanical energy input, it enables the definition of a typical seasonal wind. The surface heat and water fluxes come from the National Oceanography Centre (NOC, formerly Southampton Oceanography Centre) 1980 to 1993 atlas for net heat flux and evaporation minus precipitation [*Josey et al.*, 1998], regridded onto our own model mesh. The open boundaries include both a radiation condition and a relaxation to climatology and thus allow information to flow in and out of the domain [*Barnier et al.*, 1998]. The normal velocities as well as the temperature and salinity are restored at the northern, western, and southern open boundaries to a monthly climatology of the POP model. As discussed in the following sections, the reduced size of the model domain makes that its results are strongly determined by the lateral boundary forcing, and hence by the circulation and water mass properties of the POP model. However, we are planning on employing this regional model in the future for process-oriented studies and for Lagrangian analyses of the circulation schemes. Thus, we need a model that can be run quite fast with a variety of forcings. In addition, the numerical simulations that we carry out also include some online Lagrangian floats whose trajectories are integrated in time during the simulation and which will be used in the Lagrangian studies. This model is run for twelve years, but the simulation that is analyzed hereafter is a climatology built from the last ten years with 5-day mean outputs.

3. Hydrological Properties

All the water masses present in the Bay of Biscay and along the Iberian margin either originate in the northern Atlantic Ocean or result from interactions between North Atlantic and Mediterranean waters [e.g. *Van Aken*, 2001]. (Θ, S)-diagrams and profiles typical of these regions are presented in Figure 2. The various water masses and their thermohaline properties are rendered in an acceptable way by the model. In particular, the modeled depth and density ranges compare generally well with the ones observed. The model temperature in the mixed layer also compares very well to observations with typical values of 15 to 16°C, but the salinity is about 0.1 to 0.2 psu too high, with salinities of 35.7 instead of the observed 35.55 (Fig. 2). Some notable differences are indeed found in the water mass thermohaline properties and geographical distributions. However, most of these biases are already present in the properties of the water masses in the POP model [e.g. *Colas*, 2003; *Tréguier et al.*, 2003].

The warm and relatively salty Eastern North Atlantic Central Water (ENACW) is observed below the thermocline between about 100 and 400 m. As a subdivision of the North Atlantic Central Water (NACW), it is characterized in the area by a nearly straight band in $\Theta - S$ space, with $\Theta \geq 10.9$°C and $S \geq 35.57$, which corresponds to $\sigma_\theta \leq 27.24$ (Figure 2). It originates from two types of mode waters: the subtropical ENACW, slightly warmer and saltier, is formed along the Azores Front at about 35°N, whereas the subpolar ENACW is formed in the eastern North Atlantic north of 46°N [*Fiúza et al.*, 1998]. The thermohaline properties of ENACW are well reproduced by the model, despite a slight bias toward higher temperatures at high salinities and toward lower temperature at low salinities (Figure 2). In the model, ENACW ranges from 50 m to about 400 m, that is $\Theta \geq 10.5°C$ and $S \geq 35.55$ ($\sigma_\theta \leq 27.29$).

The lower edge of subpolar ENACW is characterized by a salinity minimum ($S \leq 35.6$) at depths ranging from 400 to 700 m. In the vicinity of the Bay of Biscay, this salinity minimum is more related to the effects of seasonal stratification and fresher coastal waters than to the influence of Subarctic Intermediate Waters located northwest of the domain and Antarctic Intermediate Waters flowing along the northwestern African margin [*Van Aken*, 2000b]. This salinity minimum is shallowest (450–500 m) and most saline ($S = 35.6$ and $\Theta < 11°C$) off western Portugal [*Fiúza et al.*, 1998; *Van Aken*, 2001]. The salinity properties of the subsurface salinity minimum water as well as its depth are well represented in the model (Figure 2c), although the temperature is about 0.5°C colder than in observations (Fig. 2b). This temperature difference results in a slight bias toward larger densities (Fig. 2a). Figures 3a–b present the climatological structure of this salinity minimum in the model and in the observations; the mean observed climatological state is taken from *Levitus et al.* [1998]. The overall structure is comparable, although the poleward freshening in the model is slightly different than that observed, with salinities a bit larger in the model than in the observations at both the northern and southern boundaries of the model domain.

Underneath starts the strong influence of MW, which is characterized by high salinities ($S \sim 36.0$) and relatively high temperatures ($\Theta \sim 10°C$). The usual density range for MW off the Iberian Peninsula is $31.85 \leq \sigma_1 \leq 32.35$, and MW is located in the depth range 600 to 1400 m [e.g. *Daniault et al.*, 1994; *Iorga and Lozier*, 1999; *Van Aken*, 2000b]. The depth and density ranges of MW in the model are satisfactory, although it is too warm and too salty compared to observations (Fig. 2): off Portugal, accepted mean temperature and salinity of the MW core are 10.5°C and 36.1 [*Fiúza et al.*, 1998], whereas in the model they are 12°C and 36.5, respectively. These biases result from the forcing at the open boundaries and had already been pointed out in the POP model, along with the proper depth range reproduced for MW [*Colas*, 2003; *Tréguier et al.*, 2003]. However, the model temperature and salinity biases compensate when computing potential densities, so that the density range of MW is still valid. Reproducing acceptable depth range and properties for MW is a known challenge for most ocean models; it is the one of the reasons why POP was chosen for the boundary forcing in this study. The properties of MW in POP at the Gibraltar outflow are quite comparable to observations [*Colas*, 2003], and the high salinity and temperature of MW further in the Atlantic likely result from a lack of vertical mixing [*Colas*, 2003]. Two cores of MW have been observed in the Gulf of Cadiz [*Daniault et al.*, 1994]: the upper, warmer and fresher core ($\sigma_1 = 31.85$) is located at about 800 m, whereas the lower core ($\sigma_2 = 32.25$) is at 1200 m. These two cores are believed to follow different paths within the Gulf of Cadiz and into the Atlantic Ocean [*Iorga and Lozier*, 1999], so that by the time MW reaches the western Iberian Peninsula the double-core structure is difficult to observe [*Daniault et al.*, 1994]. Although the temperature and salinity profiles presented in Fig. 2b and c indicate a slight dissymmetry in the properties of MW with depth, there is no clear evidence that the model reproduces two cores of MW, but instead a single core of MW at a depth of 900 to 1000 m. A similar statement was made regarding POP by *Colas* [2003].

Despite the bias toward higher temperatures and salinities, the behavior of the thermohaline properties of MW in the model is in good agreement with observations: the signal of the characteristic salinity maximum decreases slowly as MW flows poleward within the eastern boundary undercurrent because of mixing with less saline water types [*Iorga and Lozier*, 1999]. The salinity of the core of MW is 36.5 at 40°N, and it decreases steadily to 36.25 at 44.5°N. This salinity loss is comparable to the one from 36.1 to 35.9 found by *Iorga and Lozier* [1999] at the above-mentioned latitudes. In the northern part of the domain, the salinity decreases from 36.15 to 36.05 in a manner still comparable to the decrease observed by *Iorga and Lozier* [1999] from more than 35.7 to 35.65. The horizontal structure of salinity is also comparable to observations, as presented in Figure 3c–d: the isohalines are oriented similarly with a general southwest-northeast direction.

Below MW at depths exceeding 1500 m, Labrador Sea Water (LSW) is characterized by low salinities (Fig. 2b). The salinity minimum associated with LSW is located at a depth of about 1800 m and corresponds to a density $\sigma_2 = 36.88$. Figures 3e and 3f present the horizontal salinity structure at this depth in the model and in the *Levitus et al.* [1998] climatology. In the model, LSW is about 0.1 to 0.2 too fresh and 0.5°C too cold, as visible in the profiles presented in Figures 2b and 2c. Observations indicate that the salinity of LSW tends to increase in the eastern Bay of Biscay (Fig. 3f) and over the continental slope because of diapycnal and isopycnal mixing [*Paillet et al.*, 1998; *Van Aken*, 2000b]. Salinity also increases further south along the western Iberian margin [*Fiúza et al.*, 1998]. In the model, LSW propagates further east than in observations: indeed, modeled salinity remains low in the eastern part of the Bay of Biscay and does not increase eastward as is found in the observations (Figs. 3e and f). Moreover, although salinity in the model increases quickly south of 43°N, the signature of LSW is still visible along the northern Portuguese Margin: the salinity contrast between the Biscay abyssal plain and the northern Portuguese Margin is much larger in the observations than in the model (Fig. 3e–f). A possible reason for this excess of LSW could be the absence of tides in the model; in particular, there is no parameterization for the effect of internal tides.

In the deepest layers, between 2500 and 3000 m, lies the North-East Atlantic Deep Water (NEADW), characterized by a salinity maximum. It is composed of a mixture of Lower Deep Water, Iceland-Scotland Overflow Water, and LSW, and its density is $\sigma_3 = 41.42$ [*Van Aken*, 2000a]. The salinity is very comparable to observations (Fig. 2b) but the temperature is about 0.5°C too cold (Fig. 2a).

In conclusion, we find that the rendering of the mean thermohaline properties and depth ranges of water masses by the model is in reasonable agreement with observations for the average water mass properties in the area. In particular, almost all water masses are located within the proper depth and density ranges, although most of them suffer from systematic, but with respect to density, compensating biases temperature and salinity. The most striking model bias is MW being too warm and too salty; however, the modeled freshening of MW as it propagates poleward is comparable in amplitude to the one observed. Similar conclusions were reached by *Tréguier et al.* [2003] and *Colas* [2003] regarding the water masses rendered in the POP model.

4. Mean Circulation and Seasonal Cycle

The vertical structure of the circulation in the area is mostly barotropic over the abyssal plains within the upper 1500 m and highly baroclinic over the continental slope, as illustrated by the vertical sections at 42°N presented in Figure 4; in particular, Figure 4 indicates the presence of four currents trapped at the continental slope along the Iberian slope. These slope currents will be presented and discussed in more details hereafter.

The vertical structure along the slope throughout the model domain is very similar to that illustrated by Figure 4. Besides, the model simulates a strong seasonality, especially in the upper 2000 m over the continental slope, as partly illustrated by Figure 4. This variability is mainly associated with flow reversals. The details of the seasonal changes in the circulation at various depths are discussed below, with comparison to observations.

4.1. From the Surface to 300 m

4.1.1. Off the Iberian Peninsula

The circulation between 30 m and 160 m as well as the temperature field at 50 m at various moments of the year are presented in Figures 5 and 6 respectively.

In early October, a poleward jet intensifies over the upper slope in the model, extending from Portugal to north of Goban Spur (Fig. 5a). It is located in the upper 200 to 300 m (Fig. 4) and resembles the IPC [*Frouin et al.*, 1990; *Haynes and Barton*, 1990] (sometimes referred to as the Portugal Coastal Countercurrent [*Pérez et al.*, 2001]). The model jet extends from inshore of the shelf break to beyond mid-shelf, as observed by *Frouin et al.* [1990]. The core of maximum velocities is located at an average depth of 30 to 50 m slightly offshore of the shelf break (Fig. 4). *Haynes and Barton* [1990] measured the highest velocities off Portugal at depths of 100 to 200 m on average. In the model, the jet intensifies and peaks in late December-early January with maximum velocities of about 17 cm s^{-1} (Fig. 4). These values are comparable to those measured by *Haynes and Barton* [1990] who obtained maximum velocities close to 20 cm s^{-1}, or those estimated by *Frouin et al.* [1990] from satellite imagery. Also, the poleward transport computed over the width and depth range (0–200 m of the slope current associated with the phenomenon peaks at about 0.7 to 0.8 Sv off Portugal and 0.5 to 0.6 Sv off northern Spain, in very good agreement with the transport estimates obtained by *Frouin et al.* [1990] at 41°N–42°N (0.5–0.7 Sv). The slight underestimate of velocities is due to the fact that the model velocities are averaged over 5 days; instantaneous velocities locally reach up to 25 cm s^{-1}. The jet advects warm and salty waters originating off Portugal first poleward along the western Iberian shelf break, then around the northwestern corner of the Iberian Peninsula, and along the Cantabrian Slope into the Bay of Biscay, as depicted in the temperature maps at 50 m presented in Figure 6. This propagation is realistic and the warm water tongue has been detected as far as 2.5°W, even though the eastward extent of the penetration into the Bay of Biscay is subject to interannual variability [*Garcia-Soto et al.*, 2002]. The warm water tongue in the model is also in good agreement with observations: the core of warm and salty waters is centered around 100 m within the core of the jet, and narrows and weakens as it propagates poleward. Off Portugal, waters in this warm and salty tongue are typically about 1° to 1.5°C warmer and 0.1 to 0.2 psu saltier than surrounding waters (Fig. 6a).

From late winter-early spring on, the model IPC off Portugal weakens but persists in summer as an undercurrent from the southern boundary of the domain to Cape Finisterre (Figs. 4b–d). It narrows and its vertical extension also decreases: its upper boundary deepens to 20 m while its lower boundary shoals to about 150 m, with the core of maximum velocities located at about 30 m and velocities seldom exceeding 7 cm s^{-1} in summer (Fig. 4c–d). It remains trapped slightly offshore of the shelf break. These features tend to support observations off Portugal that report a subsurface northward offshore current in summer extending from 20 to 100 or 200 m, and which is occasionally referred to as the Portugal Coastal Undercurrent [*Peliz et al.*, 2002]. Along the Cantabrian slope, the model jet vanishes completely during summer and is replaced by a westward flow located beyond the lower slope (Fig. 5c). During that period typical velocities over the upper slope are about $3\,\mathrm{cm\,s^{-1}}$. *Pingree and Le Cann* [1990] found a poleward current at 200 m from October to February over the Cantabrian slope with velocities of about $10\,\mathrm{cm\,s^{-1}}$, and a weak westward flow in spring and summer.

Over the western Iberian shelf the summer circulation in the model is equatorward, with velocities up to $8\,\mathrm{cm\,s^{-1}}$ along the northern Portuguese coast (Figs. 4c and 5c). From May to September, a coastal upwelling develops along the western Iberian Peninsula, bringing colder waters (12.5°C) from 200 m deep to the surface (Fig. 6c). Such a wind-driven upwelling has been repeatedly observed off Portugal and is considered to be the northernmost part of the Canary upwelling system [*Bakun and Nelson*, 1991]. *Castro et al.* [1994] measured waters at 12°C at the Galician coast and 14°C offshore, as a result of the advection of offshore subsurface waters from depths of about 200 m. Observations in summer along the western Iberian coast evidenced an equatorward flow over the shelf east of 9.5°W with the highest velocities ($8.6\,\mathrm{cm\,s^{-1}}$) off Cape Finisterre [*Castro et al.*, 2000].

4.1.2. In the Bay of Biscay

The model circulation schemes indicate that the IPC is part of a much larger slope current system that intensifies and outcrops at the surface from fall to early spring. Indeed, the poleward surface slope current extends also over the Armorican and Celtic slopes in winter, as far north as Goban Spur at the northern boundary of the model domain (Figs. 5a). This slope current has a structure similar to that of the IPC: it extends from the surface to 200 or 300 m with its core located at about 50 m, slightly offshore of the shelf break; it ranges in the cross-shore direction from the 150-m isobath to mid-slope or beyond. Typical velocities reach about $5\,\mathrm{cm\,s^{-1}}$. Long records of velocity measurements are scarce for the Bay of Biscay, but current meters located in the vicinity of Goban Spur showed that the flow was poleward over the upper slope in winter with typical velocities of about $5\,\mathrm{cm\,s^{-1}}$ and a maximum flow in December and January [*Pingree et al.*, 1999]. This poleward surface jet over the Celtic and Armorican shelves was also found in the circulation inferred from Lagrangian drifters in the Bay of Biscay by *Van Aken* [2002] and *Colas* [2003]; *Serpette et al.* [2006]; *Le Cann et al.* [2006] with a similar range for the associated velocity estimates. As for the IPC, the surface current along the Armorican and Celtic slopes weakens, narrows, and shoals in late winter and early spring, but persists during summer as an undercurrent. It remains trapped over the shelf break but its offshore extension is greatly reduced (Fig. 5c). Its vertical extension also varies: its upper limit deepens to 20 m while its lower limit rises to 150 m. The core of maximum velocities shoals to about 30 m with velocities never exceeding $4\,\mathrm{cm\,s^{-1}}$. On the offshore flank of the slope currents the flow reverses equatorward in summer. Along the Aquitaine slope the slope current reverses from late March to early September with typical velocities of about $3\,\mathrm{cm\,s^{-1}}$ (Fig. 5b–c). In their analysis of current meter measurements along the Celtic continental slope in the vicinity of Goban Spur, *Pingree et al.* [1999] found that the summer surface circulation was weak and occasionally equatorward, especially in the upper layers.

Over the Biscay Abyssal Plain, the time variability is large compared to the mean circulation, but the modeled seasonality is much smaller than that obtained along the continental slope. Thus, there are no well-defined jets or currents but instead continuous flow whose position varies in time. Eastward flow is centered between 47° and 48°N and advects waters eastward into the Bay of Biscay from the Northeastern Atlantic Ocean (Fig. 5). The core of maximal velocities is centered around 100 m, and typical velocities vary from $3\,\mathrm{cm\,s^{-1}}$ in spring to $8\,\mathrm{cm\,s^{-1}}$ in late summer. The eastward extent of this flow varies in time: in late summer and fall, it seems to advect waters in the center of the Bay of Biscay (Fig. 5d), whereas in spring most of the flow veers northward into the Celtic slope current without entering the center of the bay (Fig. 5b). The circulation over the abyssal plain off the Cantabrian slope is characterized by several small recirculation cells centered at about 45°N (Fig. 5). On a larger scale and as a result of the winter and summer jets along the slope in the Bay of Biscay, the model surface circulation within the Bay is mainly cyclonic in winter and anticyclonic in summer.

This circulation scheme and the typical amplitude of velocities are in good agreement with the circulation inferred from surface drifters by *Pingree* [1993] and *Van Aken* [2002]: waters flow into the Bay of Biscay north of 45°N, then they flow east- to southeastward and finally exit within the poleward slope current system or as a westward current along the northern Iberian Peninsula. Based on hydrographic sections, *Paillet and Arhan* [1996] evidenced an eastward flow within the mixed layer, continuous from the eastern flank of the Mid-Atlantic Ridge to the European continental slope in the Bay of Biscay and centered at 48°N, widening and weakening as it flows eastward. The westward current along 43°N was also found by *Paillet and Arhan* [1996] from hydrographic sections and by *Paillet and Mercier* [1997] in their inverse model. Based on Lagrangian float trajectories, *Colas* [2003]; *Le Cann et al.* [2006] found that the circulation in the Bay of Biscay is composed of cyclonic and anticyclonic cells covering most of the Bay of Biscay. The cyclonic cells are mainly located in the northern part of the bay whereas the anticyclonic cell is centered north of Cape Finisterre and Cape Ortegal [*Colas*, 2003].

The circulation over the Celtic and Armorican shelves in the model is very weak and with no clear direction, except along the French coast where the flow is equatorward with velocities of about 2 cm s^{-1}. However, the model does not include any tidal forcing, which is known to be of primary importance for the mean circulation over the shelf in that region [e.g. *Puillat et al.*, 2004]. Thus the circulation obtained in the model over the Armorican and Celtic shelves should not be trusted. The absence of tidal forcing is discussed more extensively in section 6.

4.2. From 300 to 600 m

The circulation between 350 m and 520 m at various moments of the year is presented in Figure 7.

Below the poleward slope currents and undercurrents, that is from 300 to about 600 m, there is a weak and narrow (about 30 km wide) equatorward current. It is trapped at the slope and extends from 49°N to the southern boundary of the domain with some temporary and local gaps (Fig. 7). The velocities are weak, often 1 cm s^{-1} or less; it is the most intense along the Cantabrian slope where velocities can reach up to 5 cm s^{-1} intermittently (Fig. 7). The current is the most continuous in spring (Fig. 7b). In October and November the slope current reverses everywhere (Fig. 7d). These results agree partly with the observations carried out at this depth range. The slope current observed by *Pingree and Le Cann* [1990] at Cape Ortegal was weak most of the time, eastward from late September to early November and westward the rest of the year. In January and February the velocities peaked to about 10 cm s^{-1}. Moreover, *Pingree and*

Le Cann [1989] measured a poleward and persistent flow along the Celtic slope at 48°N with residual currents ranging from 3 to 6 cm s^{-1}. *Colas* [2003]; *Le Cann et al.* [2006] found that the current was mostly equatorward along the Cantabrian and Armorican slopes, but poleward along the Iberian and Celtic slope. They also observed a partial poleward flow along the Armorican and Celtic slope currents.

Offshore, between the Portugal slope and the Galicia Bank, the flow is southwestward from February to September, northwestward the rest of the year. However, the position of the southward flow seems quite sensitive to the presence of eddies, and occasionally migrates inshore or offshore by about 100 km. In particular, the southward flow appears to be pushed offshore west of the Galicia Bank from October to December when the slope currents in the upper 600 m are set poleward. Further to the west, the influence of the open boundaries and eddies is large, and it is difficult to define a clear direction for the flow. Between Portugal and the Azores Islands, observations indicate that the flow is southward and weak within the Portugal Current [*Martins et al.*, 2002]. This current is part of the southward recirculation of the North Atlantic subtropical gyre.

Over the Biscay Abyssal Plain, the circulation is quite similar to the circulation in the upper 300 m, with a strong variability and no strong jet, but instead a series of semi-persistent flow within mesoscale features. The eastward flow centered around 48°N at 14°W that was found in the upper layer (Fig. 5) is also present (Fig. 7) and advects water into the Celtic slope system. It sometimes connects to an eastward flow at 45°N eastward of 8°W (Fig. 7a and d). The westward flow along the Cantabrian slope extends into a series of west- to southwestward flows located between 43° and 46°N. Exchanges between the southern eastward flow at 45°N and the westward jet along the Cantabrian slope are occasionally possible through recirculations within anticyclonic eddies centered near 45°N–7°W (e.g. Fig. 7c). The circulation within the Bay of Biscay is mainly directed southeastward. This picture is generally consistent with the circulation obtained by *Colas* [2003]; *Le Cann et al.* [2006].

The net effect on temperature of advection by these dynamical features is depicted in Figure 8: in fall, the poleward slope current advects warm waters along the Armorican and Celtic slopes (Fig. 8a); in spring and summer however, this poleward slope current is replaced by an equatorward flow that advects colder waters along the slope (Fig. 8b).

4.3. Depth Range of Mediterranean Water

Figure 9 illustrates the salinity distribution in the core of MW in early winter and early July. The maps indicate the presence of two flows of MW off Portugal: a narrow jet is trapped at the slope, and a wider tongue flows intermittently northwestward toward the Galicia Bank. The structure of the narrow jet is illustrated by the vertical section presented in Figure 4; this jet is about 30 km wide and continuous from Portugal to Goban Spur, even though its signature in salinity drops at Cape Ortegal. It presents a strong seasonal cycle: it is poleward most of the time, but intermittently reverses or weakens so much that it vanishes, as illustrated by Figure 10. Along the western Iberian slope, it is most intense in late winter and early spring with velocities up to about $6\,\mathrm{cm\,s^{-1}}$ in March and April; it reverses from November to January, with maximal equatorward velocities of $3\,\mathrm{cm\,s^{-1}}$ in the vicinity of Cape Finisterre. The jet is slightly more variable along the Cantabrian, Armorican, and Celtic slopes: the maximal poleward velocities reach about $6\,\mathrm{cm\,s^{-1}}$ in fall (October), the flow reverses from December to February with equatorward velocities up to $3\,\mathrm{cm\,s^{-1}}$. In late spring and summer, the flow is generally poleward but weak (1 to 2 cm s^{-1} from May to August) as illustrated by Figures 10b–c. The effect of these circulation schemes is visible on the salinity maps of Figure 9: a fresher tongue propagates equatorward in winter along the Celtic, Armorican, and especially Cantabrian slopes (Fig. 9a), whereas the rest of the year a salty tongue is advected poleward (Fig. 9b).

The position of the offshore MW tongue varies throughout the year although it remains generally comprised between the coast and about 13°W. It is located in the immediate vicinity of the slope from July to October and starts moving offshore from November on when the flow in the vicinity of the Iberian slope is directed southward (Fig. 10a). As a result, the offshore MW tongue tends to move northwestward toward the Galicia Bank from fall onwards (Fig. 9a).

In their census of the various pathways for MW along the western Iberian Peninsula, *Daniault et al.* [1994] found that most of the northward transport of MW takes place in a very narrow band located just against the slope. They also identified a tongue of MW west of the Galicia Bank indicated by a clear salinity maximum that seemed to propagate northwestward. Recent experiments evidence the fact that there is a seasonal cycle in the depth range of MW [e.g. *Colas*, 2003]. Yet, *Pingree and Le Cann* [1990] only found poleward flow for MW along the Cantabrian slope with velocities of about 2 to 3 cm s^{-1}. On the other hand, *Daniault et al.* [1994] evidenced variability in the strength and direction of the MW flow along the western Iberian continental slope, with occasional flow reversals at 700 and 1000 m. In particular, one of their moorings revealed a southward flow from mid-November 1988 to late February 1989 at 700 m. *Huthnance et al.* [2002] also observed mostly poleward flows with occasional reversals, especially in late fall and early winter.

Over the abyssal plain, the modeled flow in the depth range of MW resembles that of the upper layers, with a large time variability but no strong seasonal signal. In the model, water seems to be advected eastward around 48°N close to the western boundary of the domain. In their inverse model study, *Paillet and Mercier* [1997] found a southeastward flow at 1000 m between 45°N and 47°N or so, and a westward current at the latitude of Cape Finisterre.

The model circulation also bears some resemblance with the one obtained by *Colas* [2003]; *Le Cann et al.* [2006], in particular regarding the entry into the Bay of Biscay around 47°N along with the connections between this entry point and the Celtic slope, as well as the winter-intensified westward bifurcation of MW toward the Galicia Bank. *Colas* [2003]; *Le Cann et al.* [2006] also found that the slope currents along the Aquitaine and southern Armorican slopes were very weak, and that the flow of MW was subject to seasonal variations.

4.4. Depth Range of Labrador Sea Water and Deeper

Below, at the level of LSW, the model circulation over the abyssal plain is quite similar to the one that was found in the upper layers: there is no obvious presence of strong jets, but recurrent mesoscale features allow semi-continuous flow of water that connects to pathways into the slope system of the Bay of Biscay. The time variability is high but there is no strong seasonal signal. Velocities above the abyssal plain seldom exceed $1\,\mathrm{cm\,s^{-1}}$ (Fig. 11). The model simulates a slope current, which extends over the whole domain. Although the slope current is generally directed equatorward, it varies seasonally in strength and direction. The maximal velocities are found from November to January; they reach about 4 to $6\,\mathrm{cm\,s^{-1}}$ along the Iberian and the western Cantabrian slopes,

$2\,\mathrm{cm\,s^{-1}}$ along the eastern Cantabrian slope, and 2 to $3\,\mathrm{cm\,s^{-1}}$ along the Armorican and Celtic slopes (Fig. 11a). From mid-February to late April or early May, the slope current reverses poleward; maximal velocities reach $2\,\mathrm{cm\,s^{-1}}$ along the Iberian slope, $1\,\mathrm{cm\,s^{-1}}$ or less along the Cantabrian, Armorican, and Celtic slopes. However, the slope current does not seem to be continuous in space. Another even shorter episode of poleward flow occurs from August to November, although its exact duration varies from a location to another. In addition, the slope current does not reverse everywhere. Along the Iberian slope for example, it reverses only locally, but in general weakens dramatically; neither poleward nor equatorward velocities exceed a few millimeters per second. Along the Cantabrian, Armorican, and Celtic slopes, the slope current reverses, but the maximal poleward velocities seldom exceed $1\,\mathrm{cm\,s^{-1}}$.

This circulation disagrees with the southern entry point of LSW into the Bay of Biscay obtained by *Paillet et al.* [1998] with an inverse model. However, their analysis of CTD transects evidenced an entry into the northern half of the Bay of Biscay, north of the Charcot Seamounts. It also indicated that the LSW core is not trapped at the continental slope, which tends to discard the hypothesis of penetration within a slope current. However, data within the depth range of LSW are scarce in the Bay of Biscay. In any case and as mentioned earlier in this discussion, the model yields a different average salinity field in the depth range of LSW than observations (Fig. 3e–f); this strongly suggests that the circulation is also different.

The model circulation in the Bay of Biscay at 2500 m is cyclonic, with an entry point into the Bay of Biscay south of the Biscay Seamount (45.5°N–10.5°W), and then between the Iberian Peninsula and the Charcot (45°N–13°W) Seamounts. The mean velocities are

$1\,\mathrm{cm\,s^{-1}}$. The penetration of ENADW into the Bay of Biscay is probably more efficient in summer and fall when the cyclonic cell widens eastward. The slope current along the Iberian, Cantabrian, and Aquitaine–Armorican slopes is alternatively equatorward (December to February) and poleward (March to November), with maximum velocities of $1\,\mathrm{cm\,s^{-1}}$. This circulation resembles the one computed by *Paillet and Mercier* [1997] with their inverse model: they obtained a cyclonic circulation at 2500 m in the Bay of Biscay, although it extends less far eastward than our model cell.

Underneath, the circulation has a weak seasonal cycle and mainly consists of a cyclonic recirculation around the Biscay and Charcot Seamounts, with velocities of $1\,\mathrm{cm\,s^{-1}}$ or less. The agreement with *Paillet and Mercier* [1997] is satisfactory, even though their inverse model gave a cell that penetrated further eastward into the Bay of Biscay.

5. Lagrangian analysis

We use the offline mass-preserving trajectory scheme proposed by *Blanke and Raynaud* [1997] to trace the pathways of water masses in the model. Water masses are represented by numerous small water parcels seeded on given geographical sections; each of them carries an elementary transport [*Döös*, 1995; *Blanke and Raynaud*, 1997]. Because of water incompressibility, a given particle conserves its infinitesimal mass along its trajectory. The trajectories are integrated in time until they reach given geographical interception sections. Trajectories can be computed forward or backward in time by simply reversing the sign of the velocity field and re-ordering the velocity samples. Pathways are visualized as horizontal streamfunctions obtained by the vertical integration of the 3D transport field represented by the particles displacement [*Blanke et al.*, 1999, 2001]. More generally, streamfunctions can be computed over any plane by integrating the 3D transport field along the transverse direction. The visualization of the pathways as streamfunctions may not mirror the complexity of individual trajectories but highlights the most robust features of the circulation by eliminating unnecessary trajectory details [e.g. *Friocourt et al.*, 2005].

We define three sections near the southern, northern, and western edges of the domain; in order to reduce the effect of the lateral boundaries on trajectory calculations these sections are not located exactly at the model edges but rather 0.5° inside the domain. Our Lagrangian analysis focuses exclusively on the water masses that interact with the Bay of Biscay proper. Thus, we also define a Bisc area that is limited to the west by the longitude of Cape Ortegal (8°W) and to the north by the westernmost tip of Brittany (48.5°N), and corresponds to the center of the Bay of Biscay.

In the following analysis, we integrate particles forward or backward in time from the southern section until they reach any of the three lateral sections. Then, we leave out all the particles that do not penetrate into the Bisc area; this approach enables to highlight the pathways of water masses into and out of the Bay of Biscay. Using the southernmost section as the initial section also reduces the occurrence of recirculating particles: because of the reduced size of the domain, the risk is quite large that the western boundary of the domain cuts through a recirculation cell; in such a case, the Lagrangian integration of these trajectories would give the impression of a large outflow/inflow of particles to/from the west. The approach that was chosen focuses on transfers that occur over a large enough distance that particles experience some relatively large property changes, so that the transfers can no longer be considered as recirculations.

We define four water masses with density criteria that are imposed at the southern boundary, so that only the particles that are in the corresponding density class at the southern section are integrated in time. During the integration however, the density condition is released no matter what density changes the particles might experience. The trajectories are integrated in time using the same climatological velocity fields as the ones that were described throughout the study, that is the model fields built from years 3 to 12 with 5-day mean outputs.

The first two density criteria are $\sigma_\theta < 27.25$ and $27.25 \leq \sigma_\theta, \sigma_1 \leq 31.90$. The lighter density class corresponds to upper ENACW, whereas the denser class corresponds to lower ENACW and also includes the salinity minimum water that is located at the base of ENACW. Upper ENACW flows mostly poleward within the uppermost slope current along the west European shelf. Lower ENACW flows mostly equatorward within the underlying slope current. Thus, the particles that belong to upper ENACW and lower ENACW are integrated forward and backward in time, respectively. In the density range of lower ENACW, the transfers are only equatorward, making forward integrations useless.

The Lagrangian streamfunction for the poleward export of ENACW is presented in Figure 12a. ENACW flows poleward along the Iberian slope. The particles for this transfer are everywhere within the upper 200 m. Although a fraction of the flow starts outside the Iberian slope current at 40.5°N, by the time ENACW reaches Cape Finisterre all the flow has been transferred within the Iberian Slope Current. Part of the flow veers eastward within the Cantabrian slope current while the remainder flows northward and then eastward and enters the Bay of Biscay in the interior at 45°N, within a large anticyclonic cell located north of the Cantabrian slope and extending from 10 to 2°W. However, because of the seasonal reversals that were described earlier, some additional Lagrangian diagnostics indicate that only a third of the waters within the Cantabrian slope current at 8°W reaches 5°W without turning around within this recirculation cell. East of 5°W, the Cantabrian slope current is too weak to advect water particles efficiently and most of the flow enters the recirculation cell just north of the Cantabrian slope. After some recirculations in the large aforementioned cell, about 55% of the total ENACW flow is expelled to the west and exits the domain. Most of the remainder connects at 45°N–4°W with the northwestward-flowing slope current along the Armorican and Celtic slopes. In addition, a northward route from Cape Finisterre to the Celtic slope within the interior is also possible, although it concerns a minor fraction of the flow.

This circulation scheme is quite similar to the one obtained by *Colas* [2003]; *Serpette et al.* [2006]; *Le Cann et al.* [2006] with Lagrangian floats, in particular regarding the lack of a direct entry route in the Bay of Biscay along the Cantabrian slope. Instead, the floats were seen to travel northward and enter the Bay of Biscay in the interior around 45 to 46°N, and then to flow either southeastward toward the Cantabrian slope or northeastward toward the Armorican and Celtic slopes. Numerous floats indicated exchanges between the Armorican and Celtic slope currents and the interior of the bay [*Colas*, 2003; *Serpette et al.*, 2006; *Le Cann et al.*, 2006].

The Lagrangian streamfunction for the equatorward export of ENACW and of salinity minimum water is presented in Figure 12b. The entry of these water masses into the domain takes place in the interior north of 48°N, with an additional small fraction entering the area with the (equatorward) slope current along the Celtic slope between 250 and 600 m deep. The interior flow has an overall southeastward direction and brings waters into the Bay of Biscay until about 3.5°W. Exchanges between the interior and the slope currents along the Celtic and Armorican slopes seem numerous. ENACW then flows westward along the Cantabrian slope, but only partly within a slope current. It overshoots the northwestern corner of the Iberian Peninsula and eventually turns south- to southwestward before exiting the domain at the southern section. A marginal fraction of ENACW flows equatorward along the Iberian slope between 250 and 600 m.

The third density criterion $31.90 \leq \sigma_1 < 32.30$ corresponds to the density of MW at the southern boundary; the particles within this density range are integrated forward in time and the corresponding streamfunction is presented in Figure 12c. The total transport of MW entering the Bay of Biscay in the model is 0.15 Sv, almost all of which flows within the Iberian slope current. As MW reaches the northwestern corner of the Iberian Peninsula, the inflow separates into two routes: a slope current pathway along the Cantabrian slope and an interior pathway. The latter is centered at 45°N, and is separated from the Cantabrian slope by a series of anticyclonic recirculation cells located north of Cape Ortegal. At 8°W half of the flow of MW (0.08 Sv) is located within the Cantabrian slope current, but at 5°W the fraction has decreased to a third (0.05 Sv), indicating that part of the flow has turned around within the recirculation cell centered at 45°N. In general, there are numerous connections between the Cantabrian slope current and the recirculation cells that are located just north of the northern Iberian coast, as illustrated by Figure 12c. Part of these connections might be caused by the seasonal reversals of the slope current that were described in the previous section. Both the interior and the slope pathways drive part of the flow southeastward to the corner of the Bay of Biscay in the vicinity of the Aquitaine slope. A slope current flows poleward along the Armorican and Celtic slopes and transports about 0.04 Sv (25% of the total inflow) toward the northernmost exit point at 12–13°W. However, the transport within this slope flow weakens as some recirculation cells, for instance the cell near 46°N–6°W, bring some waters back into the interior. Most of the MW flow (0.09 Sv) exits the area toward the west, mostly between 44 and 47°N. This export mostly results from water particles that recirculate in the large anticyclonic cell north of Cape Ortegal and are thereafter expelled westward.

This picture is again very comparable to the one obtained by *Bower et al.* [2002]; *Colas* [2003]; *Le Cann et al.* [2006] with Lagrangian floats. In particular, no float experienced a direct entry into the Bay of Biscay within the slope current. Instead, the floats flowed northwestward after the northwestern corner of the Iberian Peninsula and eventually veered eastward within a large anticyclonic cell located north of Cape Ortegal. The entry in the Bay of Biscay took place between 45 and 46°N [*Colas*, 2003; *Le Cann et al.*, 2006]. A fraction of this water then flows southeastward and reconnects with the Cantabrian slope. *Colas* [2003]; *Le Cann et al.* [2006] also found some large recirculation cells: the aforementioned, anticyclonic cell north of Cape Ortegal, and a cyclonic cell centered at 47°N–10°W, which connects with the Celtic slope current [*Colas*, 2003; *Le Cann et al.*, 2006].

The final density criterion $32.30 \leq \sigma_1, \sigma_2 < 36.96$ corresponds to LSW. In this case, the particles are integrated backward in time to focus on equatorward transfers that have a north-south direction. The obtained transfer is 0.15 Sv and the corresponding horizontal streamfunction is presented in Figure 12d. Of the particles that enter the Bay of Biscay, two thirds flow into the domain within an interior pathway at 48°N and the remaining third within a slope current at 14°W. The interior pathway tends to flow southeastward until 8°W and then to veer southward until the Cantabrian slope, with two anticyclonic recirculations northeast and northwest of Cape Ortegal. The slope current brings waters further into the Bay of Biscay until almost 5°W; there, the flow separates from the slope and flows generally southward with some small-scale recirculations in the southeastern corner of the bay. The flow reaches the Cantabrian slope between 5 and 6°W. From then on, most of the LSW flow is within the slope current along the western Cantabrian and Iberian slopes until 40°N. These results indicate that the slope current along the Celtic-Armorican slopes that was described in the Eulerian section of our study indeed seems to play a significant role in the LSW inflow into the Bay of Biscay. Velocities within the interior flow are weaker than within the slope current, but they span wider geographical ranges and are present throughout the year. This makes the interior route the main inflow for LSW into the bay. The Lagrangian picture raises the issue of the existence and role of the slope currents in the inflow and outflow of LSW; our model results disagree quite strongly with the results obtained by *Paillet et al.* [1998] from inverse modeling, who did not evidence any flow of LSW along the slope. Although some Lagrangian experiments were carried out in the depth range of LSW, the coverage of the Bay of Biscay within this depth range remains too scarce to yield any usable result [*Bower et al.*, 2002; *Colas*, 2003].

6. Discussion and conclusions

We investigate the seasonal cycle of the circulation along the Iberian Peninsula and in the Bay of Biscay by means of a numerical primitive equation model. The model circulation can be separated between weak interior flows and slightly more intense flows within a baroclinic slope current system. This system extends from the surface to about 2000 m and is subject to seasonal variations in strength as well as flow reversals, whereas the interior flow is more homogeneous with depth and less strongly influenced by the seasonality. The seasonal response of the slope current system varies geographically. The uppermost slope current extends throughout the upper 200 to 300 m and is mainly directed poleward. It peaks in fall and winter and weakens or even reverses in summer. Just below is a weak, mainly equatorward slope current that reverses in fall. In the depth range of MW the slope current is mainly directed poleward, but again reverses in winter. The model also simulates a slope current that flows in the depth range of LSW and is predominantly directed equatorward, although it also reverses in late winter and early spring, as well as locally in summer.

A Lagrangian numerical analysis highlights the pathways of the main water masses throughout the Bay of Biscay. It indicates that, although the slope current system is responsible for a significant fraction of the inflow into and the outflow out of the Bay of Biscay, it is unable to advect water masses in a continuous and uninterrupted way. The water masses that flow into the Bay of Biscay from the south are advected by the slope currents located along the western Iberian Peninsula, but upon reaching the northwestern corner of the peninsula they tend to overshoot and eventually flow into the bay within the interior. The Lagrangian analysis also indicates that there are numerous connections between the interior and the slope current system so that a continuous flow along the slope throughout the Bay of Biscay seems unlikely. Similar conclusions can be drawn regarding the waters that flow into the Bay of Biscay from the northwest, except that they come mostly from the interior, presumably because the (equatorward) slope current system along the Celtic slope is weaker than its (poleward) Iberian counterpart. These Lagrangian results compare generally well with the trajectories of the Lagrangian drifters that were recovered in the area [*Van Aken*, 2002; *Colas*, 2003; *Le Cann et al.*, 2006].

The geographical extent of the model domain is small, and its results are therefore greatly determined by the POP model data that are imposed at its lateral boundaries; in fact, most of the results that are presented in this study would also apply to POP [*Colas*, 2003]. However, the gain in horizontal and vertical resolution between POP and the present model, albeit small, allows narrower slope currents. In addition, the reduced domain size makes the model much more efficient to analyze and run. This ease of use allowed a model set-up in which a series of sensitivity studies was carried out; the results will be reported elsewhere.

Although this study focuses on the "large-scale" features of the circulation, the spatial scales of the slope currents require a relatively fine horizontal resolution. Yet, the model resolution (1/15°) is too coarse to allow more than a partial resolution of the (sub)mesoscale activity; in particular, tests in a channel model carried out specifically for the Iberian Slope region suggest that a horizontal resolution of 1/48° is needed for generating realistic upwelling filaments in this region [*Stevens et al.*, 2000]. Although the resolution of our model is also slightly too coarse to simulate narrow currents, it is fine enough to simulate slope currents with acceptable transports. The western Iberian Peninsula and the southern Bay of Biscay are also regions where (sub)mesoscale activity plays a significant role: formations of so-called meddies have been observed at least at two locations in southwestern Portugal [e.g. *Bower et al.*, 1997], and the Cape Finisterre–Cape Ortegal area is also suspected to be a formation site [e.g. *Paillet et al.*, 2002]. In the Bay of Biscay, some eddies have been repeatedly observed along the Cantabrian slope west of about 4°W, thus indicating the presence of at least one formation site in the area [e.g. *Pingree and Le Cann*, 1992; *Garcia-Soto et al.*, 2002; *Serpette et al.*, 2006]. Although shedding of such eddies may take place during preferred seasons, it seems to be a robust feature of the circulation in the area. In all cases, it should be kept in mind that the circulation is far from being as smooth as the descriptions made in sections 4 and 5 might suggest. In a similar way, because our analysis was carried out on climatological fields, our results do not take into account any interannual variability in the circulation. Yet satellite observations from 1979 to 2000 evidenced a strong interannual variability of the Navidad phenomenon, and especially of the eastward extent of the warm water tongue along the Cantabrian slope [*Garcia-Soto et al.*, 2002].

The resolution of the model makes it difficult to run on a domain larger than the current regional area; this implies forcing at the lateral boundaries in addition to forcing at the surface. Implementing proper open boundary conditions is a difficult problem to which no universal solution has yet been found. Although our model was run with mixed open boundary conditions that allow disturbances to radiate out of the domain [*Barnier et al.*, 1998], it turns out that eddies do not exit the domain immediately after they reach a boundary, but persist for a few months. However, this problem seems to appear only within about one degree of the western, northern, and southern open boundaries. Most currents and features discussed in this study are located outside of this 1°-edge.

Tides are important in the area, in particular in the Bay of Biscay north of 45°N. Indeed, the slope of the topography as well as the broadness of the Celtic shelf increase the effect of tides; thus the surface tidal forcing on the Celtic shelf is of the same order of magnitude as the wind forcing [e.g. *Huthnance*, 1995]. Further offshore, interaction of the surface tide with the shelf break causes internal tides, which can in turn greatly enhance mixing when the internal tide amplitude is large enough [*New*, 1988]. As tidal forcing was not included in the simulation, the model misses a key-element for reproducing a realistic circulation on the Celtic and Armorican shelves. South of 45°N, the shelf is less broad and/or the continental slope less steep, thus the response to tidal forcing is reduced. We are confident that the bias in the model circulation over the abyssal plains and the continental slope is negligible, especially as the model is generally able to reproduce both the observed winter and summer circulation patterns. Whether mixing by internal tides reaches depths of 1000 m or more is still uncertain and one may wonder whether the absence of parameterization for this physical process is a serious shortcoming. The steady decrease in the salinity maximum as MW flows poleward along the slope happens to be very comparable to the decrease observed by *Iorga and Lozier* [1999], though MW is too salty overall. This result strongly suggests that, at least in the depth range of MW, there is no mixing "missing" in the model. However, the question remains open for the upper 200 to 300 m. It is likely that tidal forcing would alter the thermohaline properties of some of the model water masses.

A numerical simulation carried out without any thermodynamical air-sea fluxes at the surface indicates that most of the features presented in the present study remain valid when such fluxes are omitted. In particular, heat and freshwater fluxes at the surface affect almost exclusively the circulation within the upper 300 m and leave the rest of the water column unaltered. In this uppermost layer, surface fluxes tend to enhance the poleward component of the slope flow, thus increasing (resp. decreasing) velocities when the slope current is poleward (resp. equatorward). The seasonal cycle of the slope currents remains however almost unmodified.

The present analysis gives a new and comprehensive numerical insight of the circulation off the western Iberian Peninsula and in the Bay of Biscay. The strong seasonality simulated by the model raises the question of the renewal of waters within the Bay of Biscay: whereas connections within the interior between the Bay of Biscay and the Atlantic Ocean are mostly persistent throughout the year, connections within slope currents seem to take place only during preferred seasons. In particular, part of MW is thought to flow poleward along the western European slope until at least Porcupine Bank [*Arhan et al.*, 1994; *Van Aken and Becker*, 1996]; although our model results tend to support this hypothesis, they also suggest that such a poleward flow would not take place continuously along the slope, but instead would involve some exchanges with the interior in the Bay of Biscay. *Bower et al.* [2002]; *Colas* [2003]; *Le Cann et al.* [2006] reached a similar conclusion when analyzing Lagrangian float trajectories. The seasonality of the model circulation also suggests that this poleward flow in the depth range of MW, and more generally any transfer that flows partly within the slope current system, might take place at preferred seasons depending on the connections between the various parts of the system. Similarly, the seasonality of the flow probably has consequences on the cross-shelf exchange in the area. In particular, the analysis of Lagrangian drifter trajectories led *Van Aken* [2002] to conclude that the continental shelf off western France is predominantly flushed in winter with waters from the (poleward) slope current. As the seasonality simulated by the model bears reasonable resemblance to the seasonal variability that is observed in the area, this model opens up possibilities of process-oriented studies aiming at a better understanding of the seasonal variability of the circulation.

Acknowledgments. Support for this study has been provided by the Délégation Générale pour l'Armement (DGA) for YF, by a grant from the Etablissement Principal du Service Hydrographique et Océanographique de la Marine (EPSHOM) (00.87.098.00.470.29.25) for BL, by the Université de Bretagne Occidentale (UBO) for SS, the Centre National de la Recherche Scientifique (CNRS) for BB, and by the Royal Netherlands Meteorological Institute (KNMI) for SD. Simulations were performed with the computational resources available at LPO, at the Centre de Brest of IFREMER, and at the CNRS Institut du Développement et des Ressources en Informatique Scientifique.

References

Arhan, M., A. Colin de Verdière, and L. Mémery, The eastern boundary of the subtropical North Atlantic, *J. Phys. Oceanogr.*, *24*, 1295–1316, 1994.

Bakun, A., and C. S. Nelson, The seasonal cycle of wind-stress curl in subtropical eastern boundary current regions, *J. Phys. Oceanogr.*, *21*, 1815–1834, 1991.

Barnier, B., P. Marchesiello, A. P. de Miranda, J. M. Molines, and M. Coulibaly, A sigma-coordinate primitive equation model for studying the circulation in the South Atlantic. Part I: Model configuration with error estimates, *Deep-Sea Res.*, *45*, 543–572, 1998.

Blanke, B., and P. Delécluse, Variability of the tropical Atlantic Ocean simulated by a general circulation model with two different mixed layer physics, *J. Phys. Oceanogr.*, *23*, 1363–1388, 1993.

Blanke, B., and S. Raynaud, Kinematics of the Pacific Equatorial Undercurrent: an Eulerian and Lagrangian approach from GCM results, *J. Phys. Oceanogr.*, *27*, 1038–1053, 1997.

Blanke, B., M. Arhan, G. Madec, and S. Roche, Warm water paths in the equatorial Atlantic as diagnosed with a general circulation model, *J. Phys. Oceanogr.*, *29*, 2753–2768, 1999.

Blanke, B., S. Speich, G. Madec, and K. Döös, A global diagnostic of interocean mass transfers, *J. Phys. Oceanogr.*, *31*, 1623–1632, 2001.

Bower, A. S., L. Armi, and I. Ambar, Lagrangian observations of meddy formation during a Mediterranean Undercurrent seeding experiment, *J. Phys. Oceanogr.*, *27*, 2545–2575, 1997.

Bower, A. S., B. Le Cann, T. Rossby, W. Zenks, J. Gould, K. Speer, P. L. Richardson, M. D. Prater, and H.-M. Zhang, Directly measured mid-depth circulation in the northeastern North Atlantic Ocean, *Nature*, *419*, 603–607, 2002.

Castro, C. G., F. F. Pérez, X. A. Alvarez-Salgado, G. Rosón, and A. F. Ríos, Hydrographic conditions associated with the relaxation of an upwelling event off the Galician coast (NW Spain), *J. Geophys. Res.*, *99*(C3), 5135–5147, 1994.

Castro, C. G., F. F. Pérez, X. A. Alvarez-Salgado, and F. Fraga, Coupling between the thermohaline, chemical and biological fields during two contrasting upwelling events off the NW Iberian Peninsula, *Continental Shelf Res.*, *20*, 189–210, 2000.

Coelho, H. S., R. J. J. Neves, M. White, P. C. Leitão, and A. J. Santos, A model for ocean circulation on the Iberian coast, *J. Mar. Sys.*, *32*, 153–179, 2002.

Colas, F., Circulation et dispersion lagrangiennes en Atlantique Nord-Est, Ph.D. thesis, Université de Bretagne Occidentale, Brest, France, 266 pp., 2003.

Daniault, N., J. P. Mazé, and M. Arhan, Circulation and mixing of Mediterranean Water west of the Iberian Peninsula, *Deep-Sea Res., Part 1*, *41*, 1685–1714, 1994.

Döös, K., Interocean exchange of water masses in the southern ocean, *J. Geophys. Res.*, *100*, 13,499–13,514, 1995.

Fiúza, A. F. G., M. Hamann, I. Ambar, G. D. del Rio, N. González, and J. M. Cabanas, Water masses and their circulation off western Iberia during May 1993, *Deep-Sea Res., Part 1*, *45*, 1127–1160, 1998.

Friocourt, Y., S. Drijfhout, B. Blanke, and S. Speich, Water mass export from Drake Passage to the Atlantic, Indian, and Pacific Oceans: A Lagrangian model analysis, *J. Phys. Oceanogr.*, *35*, 1202–1222, 2005.

Frouin, R., A. F. G. Fiúza, I. Ambar, and T. J. Boyd, Observations of a poleward surface current off the coasts of Portugal and Spain during winter, *J. Geophys. Res.*, *95*(C1), 679–691, 1990.

Garcia-Soto, C., R. D. Pingree, and L. Valdés, Navidad development in the southern Bay of Biscay: Climate change and swoddy structure from remote sensing and in situ measurements, *J. Geophys. Res.*, *107*(C8), 3118, doi:10.1029/2001JC001012, 2002.

Haynes, R., and E. D. Barton, A poleward flow along the Atlantic coast of the Iberian Peninsula, *J. Geophys. Res.*, *95*(C7), 11,425–11,441, 1990.

Haynes, R., E. D. Barton, and I. Pilling, Development, persistence, and variability of upwelling filaments off the Atlantic coast of the Iberian Peninsula, *J. Geophys. Res.*, *98*(C12), 22,681–22,692, 1993.

Huthnance, J. M., Circulation, exchange and water masses at the ocean margin: the role of physical processes at the shelf edge, *Prog. Oceanogr.*, *35*, 353–431, 1995.

Huthnance, J. M., H. M. Van Aken, M. White, E. D. Barton, B. Le Cann, E. F. Coelho, E. A. Fanjul, P. Miller, and J. Vitorino, Ocean margin exchange – water flux estimates, *J. Mar. Sys.*, *32*, 107–137, 2002.

Iorga, M. C., and M. S. Lozier, Signatures of the Mediterranean outflow from a North Atlantic climatology, 1. Salinity and density fields, *J. Geophys. Res.*, *104*, 25,985–26,009, 1999.

Josey, S. A., E. C. Kent, and P. K. Taylor, *The Southampton Oceanography Centre (SOC) ocean/atmosphere heat, momentum and freshwater flux atlas*, Southampton Oceanography Centre Report 6, 30pp., 1998.

Le Cann, B., K. A. Speer, A. Serpette, J. Paillet, and T. Reynaud, Lagrangian observations in the intergyre North-East Atlantic during the ARCANE and EUROFLOAT projects: Early results, *WOCE Int. Newslett.*, *34*, 25–27, 1999.

Le Cann, B., F. Colas, and A. Serpette, Mean and seasonal circulation near the eastern boundary of the mid-latitude North Atlantic Ocean, *in preparation*, 2006.

Levitus, S. E., T. P. Boyer, M. E. Conkright, T. O'Brien, J. Antonov, C. Stephens, L. Stathoplos, D. Johnson, and R. Gelfeld, *World Ocean Database 1998, volume 1: Introduction*, NOAA Atlas NESDIS 18, U.S. Department of Commerce, Washington, D.C., 1998.

Madec, G., P. Delecluse, M. Imbard, and C. Lévy, OPA 8.1 Ocean General Circulation Model reference manual, *Tech. Rep. N*°11, Institut Pierre-Simon Laplace (IPSL), France, Note du Pôle de Modélisation, 91pp, 1998.

Martins, C. S., M. Hamann, and A. F. G. Fiúza, Surface circulation in the eastern North Atlantic, from drifters and altimetry, *J. Geophys. Res.*, *107*(C12), 3217, doi: 10.1029/2000JC000345, 2002.

New, A. L., Internal tidal mixing in the Bay of Biscay, *Deep-Sea Res.*, *35*, 691–709, 1988.

Paillet, J., and M. Arhan, Oceanic ventilation in the eastern North Atlantic, *J. Phys. Oceanogr.*, *26*, 2036–2052, 1996.

Paillet, J., and H. Mercier, An inverse model of the eastern North Atlantic general circulation and thermocline ventilation, *Deep-Sea Res., Part 1*, *44*, 1293–1328, 1997.

Paillet, J., M. Arhan, and M. S. McCartney, Spreading of Labrador Sea Water in the eastern North Atlantic, *J. Geophys. Res.*, *103*(C5), 10,223–10,239, 1998.

Paillet, J., B. Le Cann, X. J. Carton, Y. Morel, and A. Serpette, Dynamics and evolution of a northern meddy, *J. Phys. Oceanogr.*, *32*, 55–79, 2002.

Peliz, A., T. L. Rosa, A. M. P. Santos, and J. L. Pissarra, Fronts, jets, and counter-flows in the Western Iberian upwelling system, *J. Mar. Sys.*, *35*, 61–77, 2002.

Peliz, A., J. Dubert, D. B. Haidvogel, and B. Le Cann, Generation and unstable evolution of a density-driven eastern poleward current: the Iberian Poleward Current, *J. Geophys. Res.*, *108*, 3268, doi:10.1029/2002JC001443, 2003.

Pérez, F. F., C. G. Castro, X. A. Alvarez-Salgado, and A. F. Ríos, Coupling between the Iberian basin-scale circulation and the Portugal boundary current system: a chemical study, *Deep-Sea Res., Part 1*, *48*, 1519–1533, 2001.

Pichon, A., Présentation et analyse des données d'hydrologie de la campagne MINT94, *Tech. Rep. 009/97*, EPSHOM/CMO/RE, 1997.

Pingree, R. D., Flow of surface waters to the west of the British Isles and in the Bay of Biscay, *Deep-Sea Res., Part 2*, *40*, 369–388, 1993.

Pingree, R. D., and B. Le Cann, Celtic and Armorican slope and shelf residual currents, *Prog. Oceanogr.*, *23*, 303–338, 1989.

Pingree, R. D., and B. Le Cann, Structure, strength and seasonality of the slope currents in the Bay of Biscay region, *J. Marine Biological Association U.K.*, *75*, 857–885, 1990.

Pingree, R. D., and B. Le Cann, Anticyclonic Eddy X91 in the southern Bay of Biscay, May 1991 to February 1992, *J. Geophys. Res.*, *97*(C9), 14,353–14,367, 1992.

Pingree, R. D., B. Sinha, and C. R. Griffiths, Seasonality of the European slope current (Goban Spur) and ocean margin exchange, *Continental Shelf Res.*, *19*, 929–975, 1999.

Puillat, I., P. Lazure, A. M. Jégou, L. Lampert, and P. I. Miller, Hydrographical variability on the French continental shelf in the Bay of Biscay, during the 1990s, *Continental Shelf Res.*, *24*, 1143–1163, 2004.

Reynaud, T., P. Legrand, H. Mercier, and B. Barnier, A new analysis of hydrographic data in the Atlantic and its application to an inverse modelling study, *WOCE Int. Newslett.*, *32*, 29–31, 1998.

Roullet, G., and G. Madec, Salt conservation, free surface, and varying levels: a new formulation for ocean general circulation models, *J. Geophys. Res.*, *105*(C10), 23,927–23,942, 2000.

Serpette, A., B. Le Cann, and F. Colas, Lagrangian circulation of the North Atlantic Central Water over the abyssal plain and continental slopes of the Bay of Biscay: description of selected mesoscale features, *Scientia Marina*, *70*, 27–42, 2006.

Smith, R. D., M. E. Maltrud, F. O. Bryan, and M. W. Heche, Numerical simulation of the North Atlantic Ocean at 1/10°, *J. Phys. Oceanogr.*, *30*, 1532–1561, 2000.

Stevens, I., M. Hamann, J. A. Johnson, and A. F. G. Fiúza, Comparisons between a fine resolution model and observations in the Iberian shelf-slope region, *J. Mar. Sys.*, *26*, 53–74, 2000.

Tréguier, A. M., C. Talandier, and S. Theetten, Modelling Mediterranean Water in the North-East Atlantic, *Tech. Rep. 02-14*, Laboratoire de Physique des Océans, UMR 6523 CNRS/IFREMER/UBO, IFREMER, BP 70, 29280 Plouzané, France, 2003.

Van Aken, H. M., The hydrography of the mid-latitude northeast Atlantic Ocean I: The deep water masses, *Deep-Sea Res., Part 1*, *47*, 757–788, 2000a.

Van Aken, H. M., The hydrography of the mid-latitude northeast Atlantic Ocean II: The intermediate water masses, *Deep-Sea Res., Part 1*, *47*, 789–824, 2000b.

Van Aken, H. M., The hydrography of the mid-latitude northeast Atlantic Ocean III: The subducted thermocline water masses, *Deep-Sea Res., Part 1*, *48*, 237–267, 2001.

Van Aken, H. M., Surface currents in the Bay of Biscay as observed with drifters between 1995 and 1999, *Deep-Sea Res., Part 1*, *49*, 1071–1086, 2002.

Van Aken, H. M., and G. Becker, Hydrography and through-flow in the north-eastern North Atlantic Ocean: The NANSEN project, *Prog. Oceanogr.*, *38*, 297–346, 1996.

Figure 1. Map of the northeastern Atlantic Ocean. The model domain is indicated by the dashed rectangle. The major geographic locations and features are labeled. The isobath 100 m, 200 m, 500 m, and 3000 m are shown.

Figure 2. Mean climatological (Θ, S) properties in the model (solid) compared to the *Reynaud et al.* [1998] climatological dataset (dashed): a) mean temperature and b) mean salinity profiles over the Biscay abyssal plain; c) (Θ, S)-diagram over the Biscay abyssal plain; the density ranges of ENACW, MW, and LSW are shaded.

Figure 3. Mean climatological maps of salinity in the model (left) compared to *Levitus et al.* [1998] (right) at: a)–b) 500 m, c)–d) 1000 m, and e)–f) 1750 m. The 100-m, 200-m, 1000-m, 2000-m, and 4000-m bathymetry contours are also indicated.

Figure 4. Zonal section of meridional velocity (in $\mathrm{m\,s^{-1}}$) at 42°N at 3-month time intervals: a) early January; b) early April; c) early July; e) late September. The depth scale is dilated in the upper 400 m. The solid (resp. dashed) contours indicate poleward (resp. equatorward) velocities; the velocity contour interval is $2\,\mathrm{cm\,s^{-1}}$ and contouring starts at $1\,\mathrm{cm\,s^{-1}}$. The dotted line corresponds to the zero-velocity contour. Velocities larger than $5\,\mathrm{cm\,s^{-1}}$ (both poleward and equatorward) are shaded.

Figure 5. Snapshots of climatological velocity vectors averaged in depth between 30 m and 160 m at 3-month time intervals: a) late December; b) early April; c) early July; d) late September. Velocities smaller than $0.2\,\mathrm{cm\,s^{-1}}$ are not shown.

Figure 6. Snapshots of climatological temperature at 50 m depth at 3-month time intervals: a) mid-January; b) mid-April; c) mid-July; d) mid-October.

Figure 7. Snapshots of climatological velocity vectors averaged in depth between 350 m and 520 m at 3-month time intervals: a) mid-February; b) mid-May; c) mid-August; d) mid-November. Velocities smaller than $0.2\,\mathrm{cm\,s^{-1}}$ are not shown.

Figure 8. Snapshots of climatological temperature at 500 m at 6-month time intervals: a) early January; b) early July.

Figure 9. Snapshots of climatological salinity at 910 m at 6-month time intervals: a) early January; b) early July.

Figure 10. Snapshots of climatological velocity vectors averaged in depth between 750 m and 1000 m at 3-month time intervals: a) mid-January; b) mid-April; c) mid-July; d) mid-October. Velocities smaller than 0.2 cm s^{-1} are not shown.

Figure 11. Snapshots of climatological velocity vectors averaged in depth between 1400 m and 1600 m at 6-month time intervals: a) early January; b) early July. Velocities smaller than 0.2 cm s^{-1} are not shown.

Figure 12. Lagrangian streamfunctions; a) for the poleward transfer of ENACW, b) for the equatorward transfer of ENACW and salinity minimum water, c) for the poleward transfer of MW , d) for the equatorward transfer of LSW. In all cases, only the particles that penetrate into the Bay of Biscay are kept; the streamfunction contour is 0.02 Sv and the 100-m, 200-m, 500-m, 1000-m, and 2000-m bathymetry contours are also indicated. The dashed lines indicate the boundaries of the BISC domain, and the arrows indicate the directions of the flow at the southern boundary.

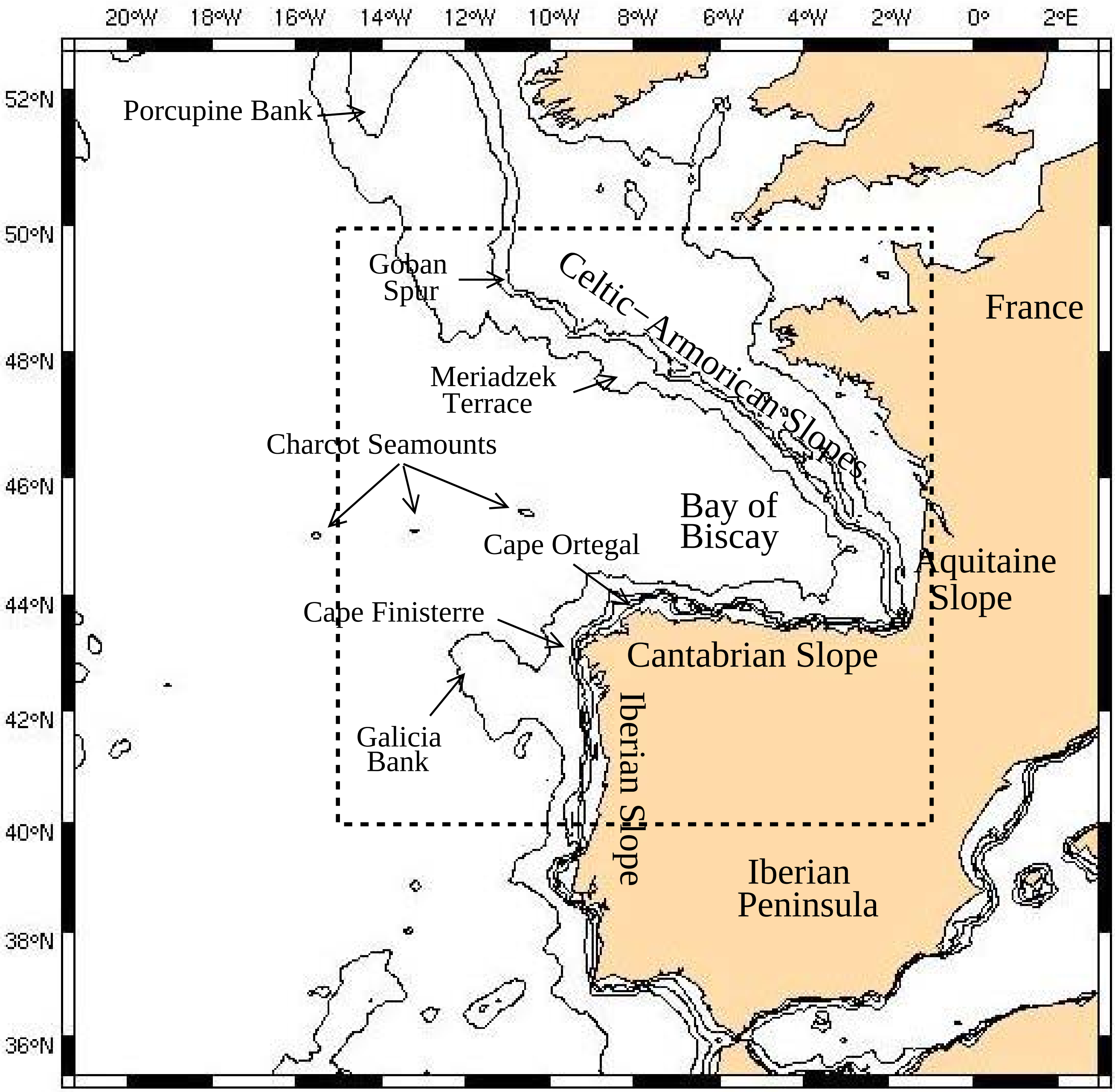

20°W
18°W
16°W
14°W
12°W
10°W
8°W
6°W
4°W
2°W
0°
2°E
52°N
50°N
48°N
46°N
44°N
42°N
40°N
38°N
36°N
Porcupine Bank
Goban Spur
Celtic–Armorican Slopes
France
Meriadzek Terrace
Charcot Seamounts
Bay of Biscay
Cape Ortegal
Aquitaine Slope
Cape Finisterre
Cantabrian Slope
Galicia Bank
Iberian Slope
Iberian Peninsula

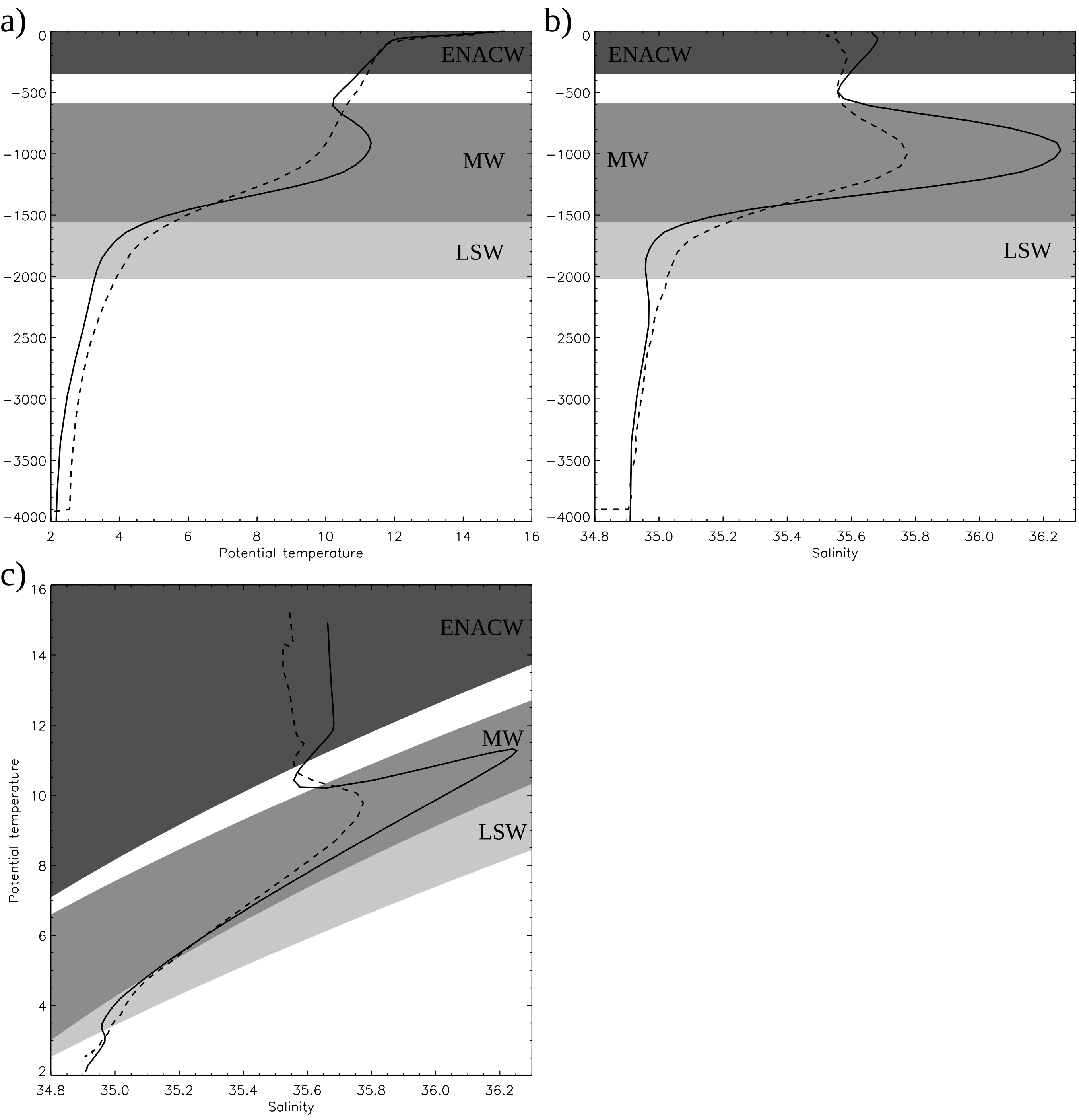
a)
ENACW
MW
LSW
Potential temperature
b)
ENACW
MW
LSW
Salinity
c)
ENACW
MW
LSW
Potential temperature
Salinity

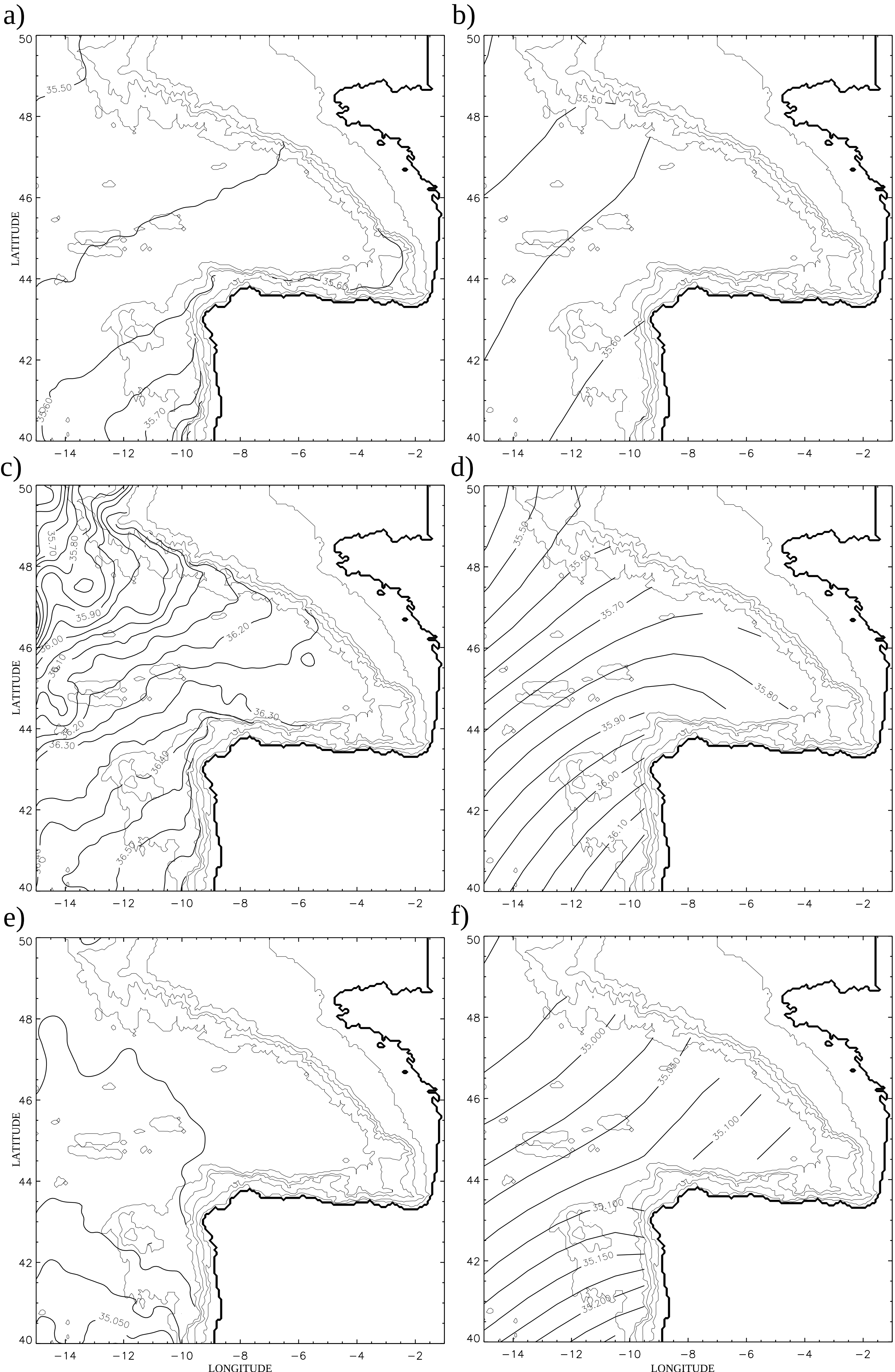

a)
b)
c)
d)
e)
f)
LATITUDE
LONGITUDE
35.50
35.60
35.70
35.80
35.90
36.00
36.10
36.20
36.30
36.40
36.50
35.000
35.050
35.100
35.150
35.200

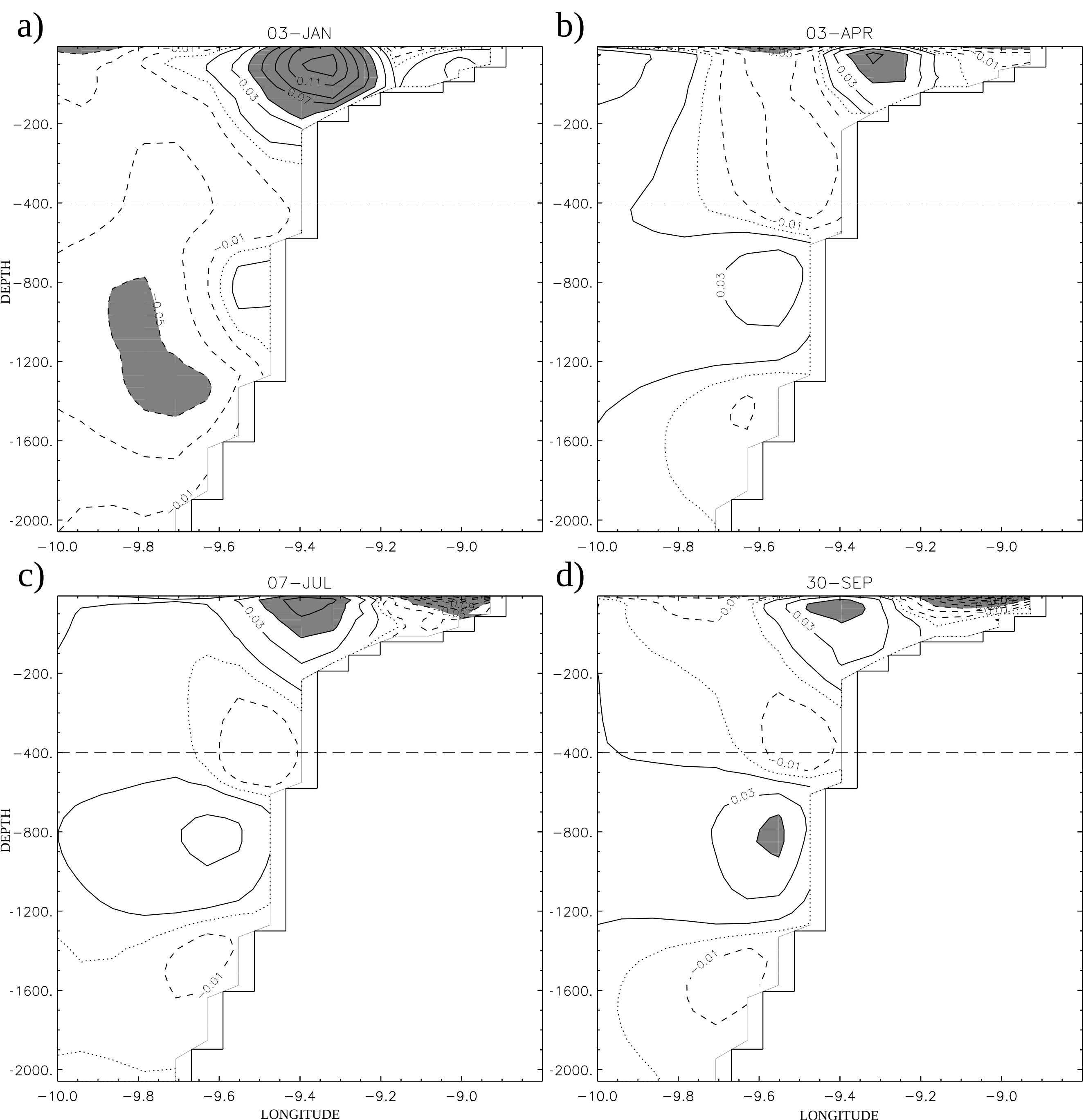
a)
03-JAN
b)
03-APR
c)
07-JUL
d)
30-SEP
DEPTH
LONGITUDE
-200.
-400.
-800.
-1200.
-1600.
-2000.
-10.0
-9.8
-9.6
-9.4
-9.2
-9.0
0.11
0.07
0.03
-0.01
-0.05
0.05
-0.0

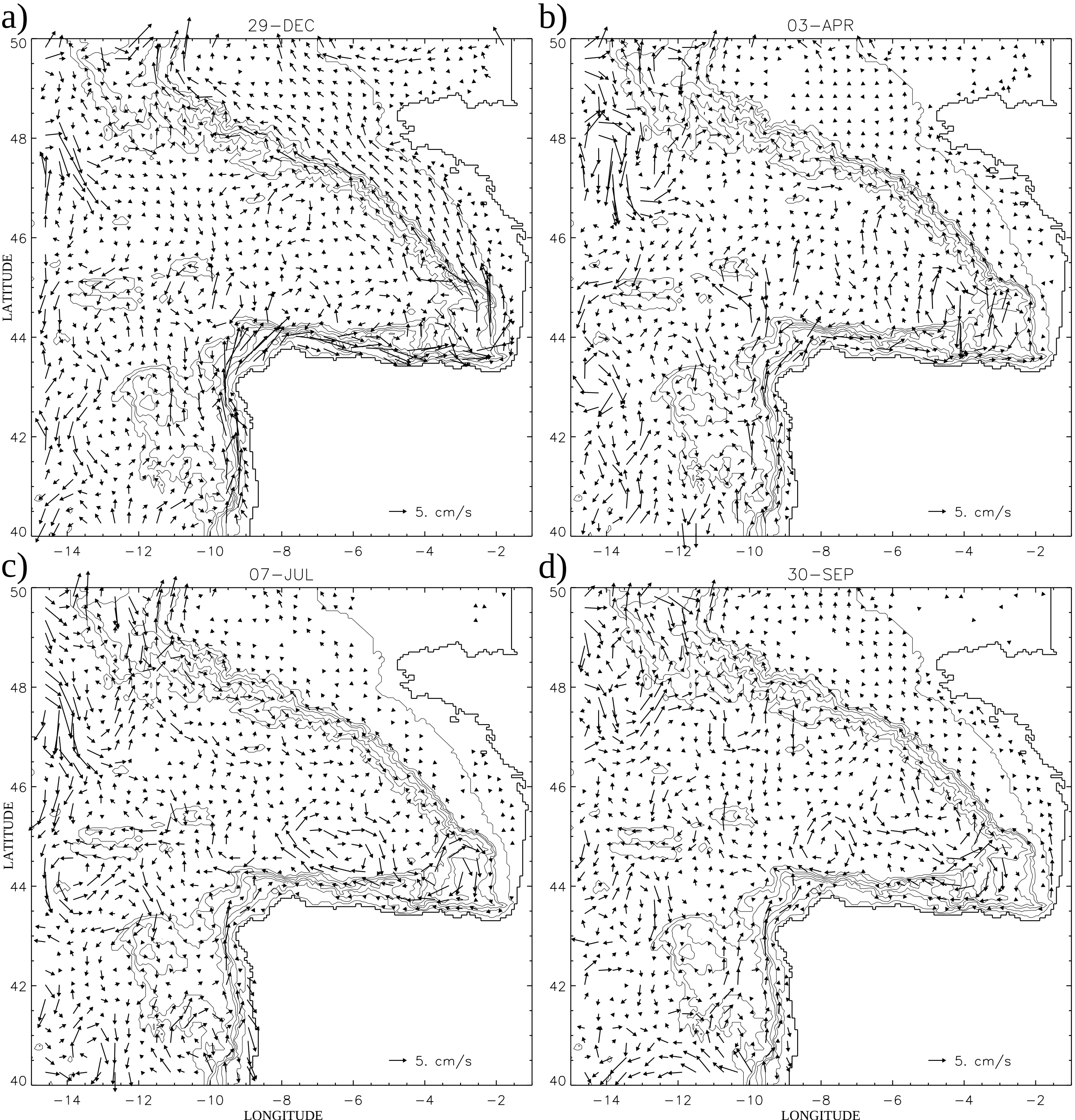

a)
29-DEC
b)
03-APR
c)
07-JUL
d)
30-SEP
LATITUDE
LONGITUDE
5. cm/s

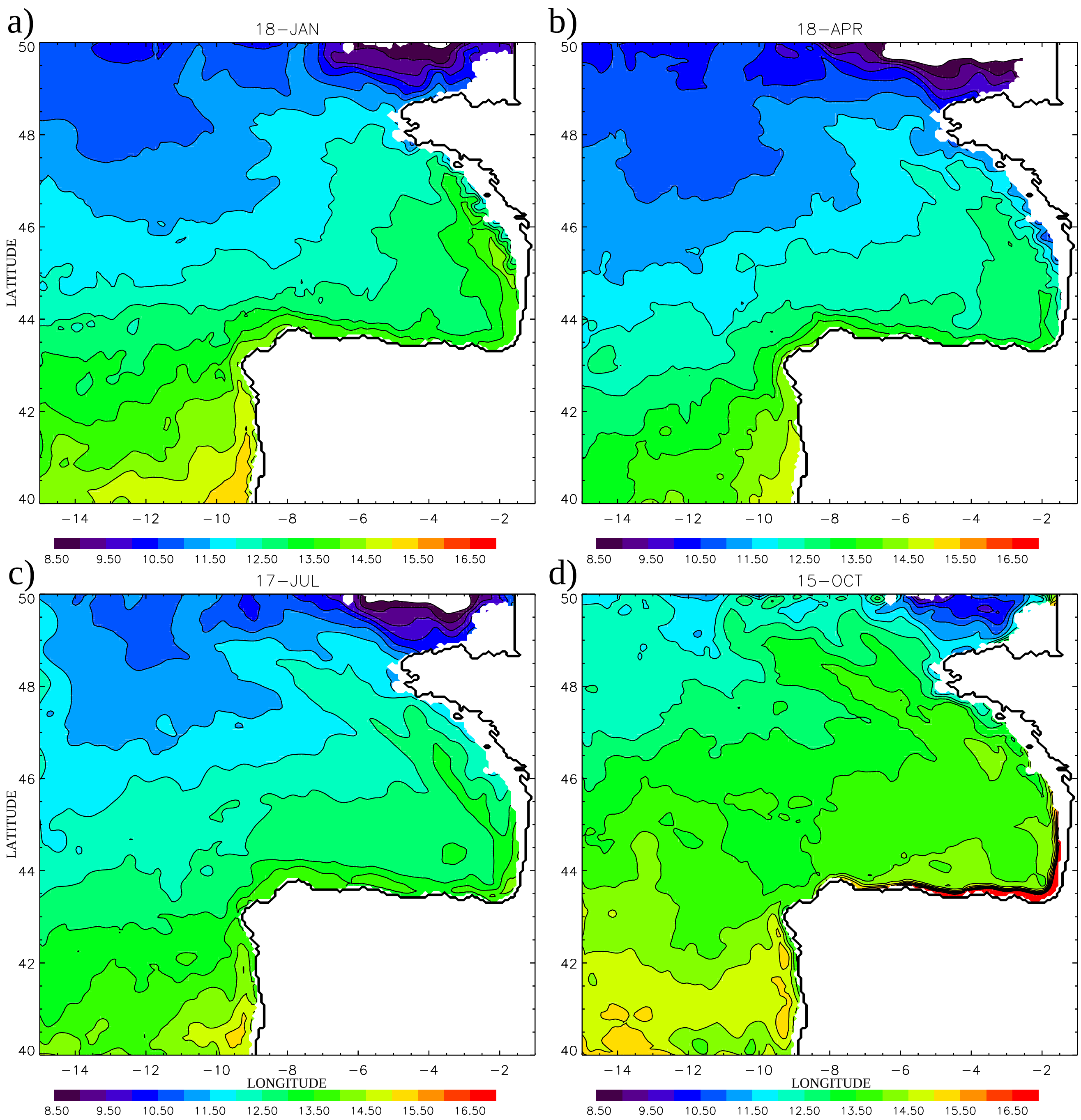
a)
18−JAN
b)
18−APR
c)
17−JUL
d)
15−OCT
LATITUDE
LONGITUDE
50
48
46
44
42
40
−14
−12
−10
−8
−6
−4
−2
8.50
9.50
10.50
11.50
12.50
13.50
14.50
15.50
16.50

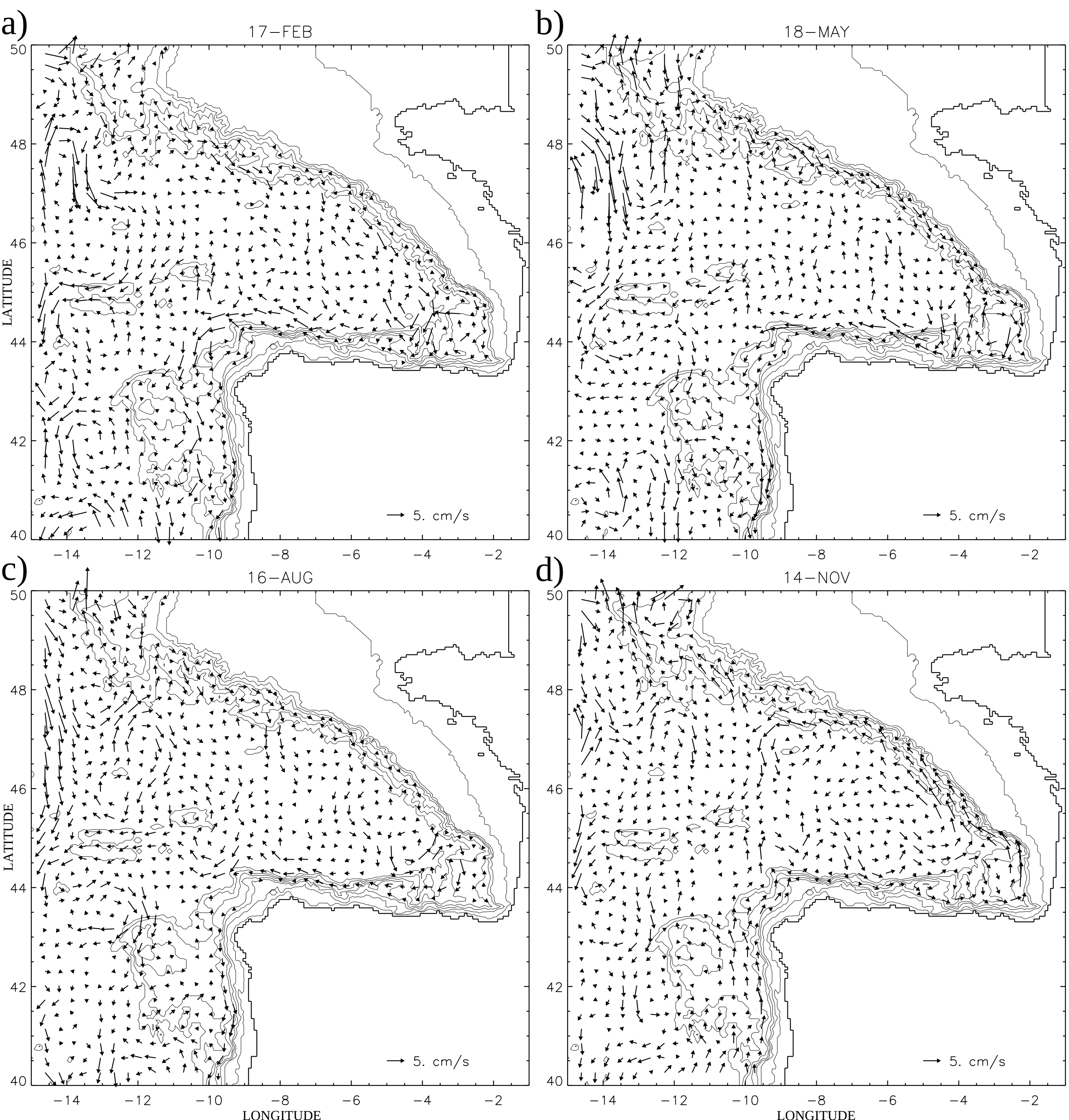

a)
17−FEB
b)
18−MAY
c)
16−AUG
d)
14−NOV
LATITUDE
LONGITUDE
5. cm/s
50
48
46
44
42
40
−14
−12
−10
−8
−6
−4
−2

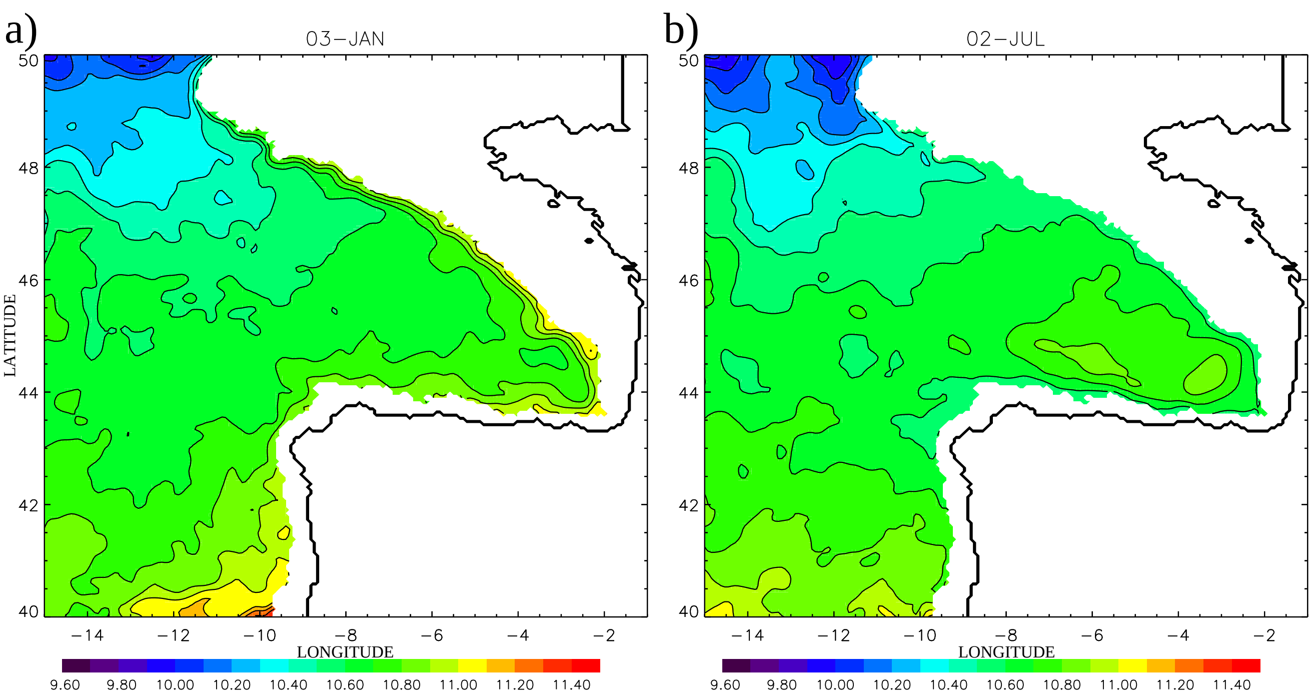

a)
03-JAN
b)
02-JUL
LATITUDE
LONGITUDE
50
48
46
44
42
40
-14
-12
-10
-8
-6
-4
-2
9.60
9.80
10.00
10.20
10.40
10.60
10.80
11.00
11.20
11.40

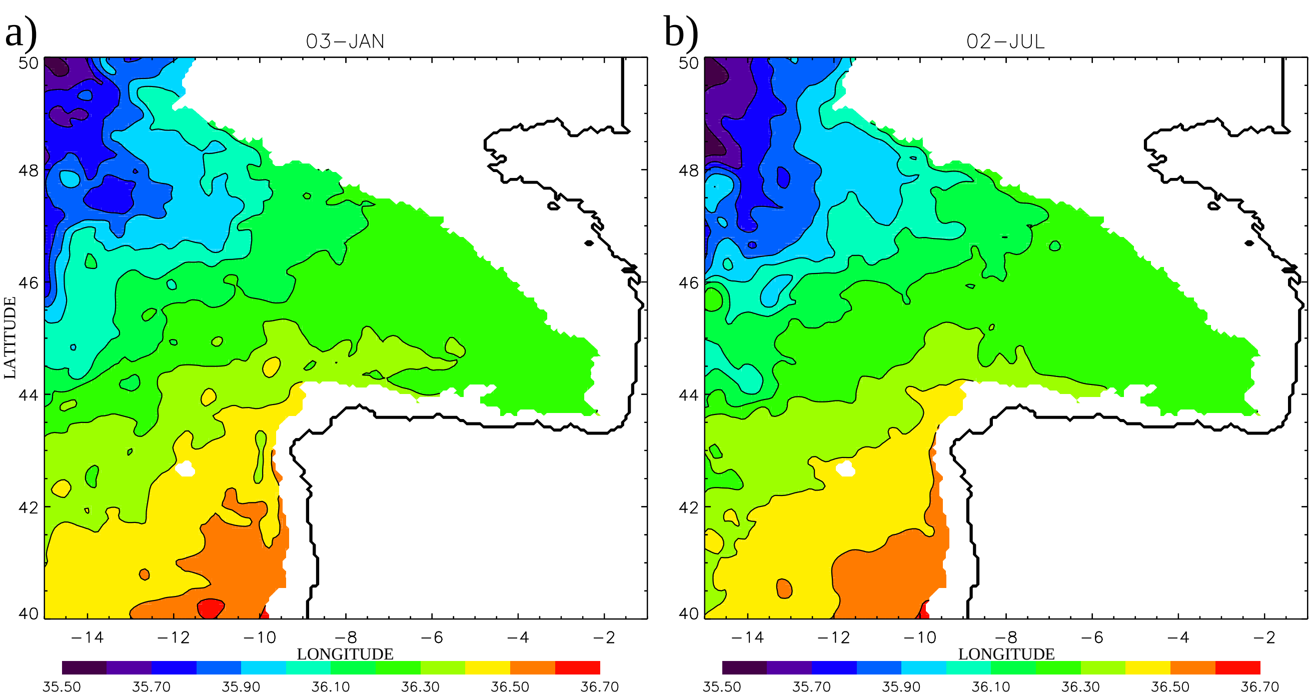
a)
03–JAN
b)
02–JUL
LATITUDE
LONGITUDE
50
48
46
44
42
40
–14
–12
–10
–8
–6
–4
–2
35.50
35.70
35.90
36.10
36.30
36.50
36.70

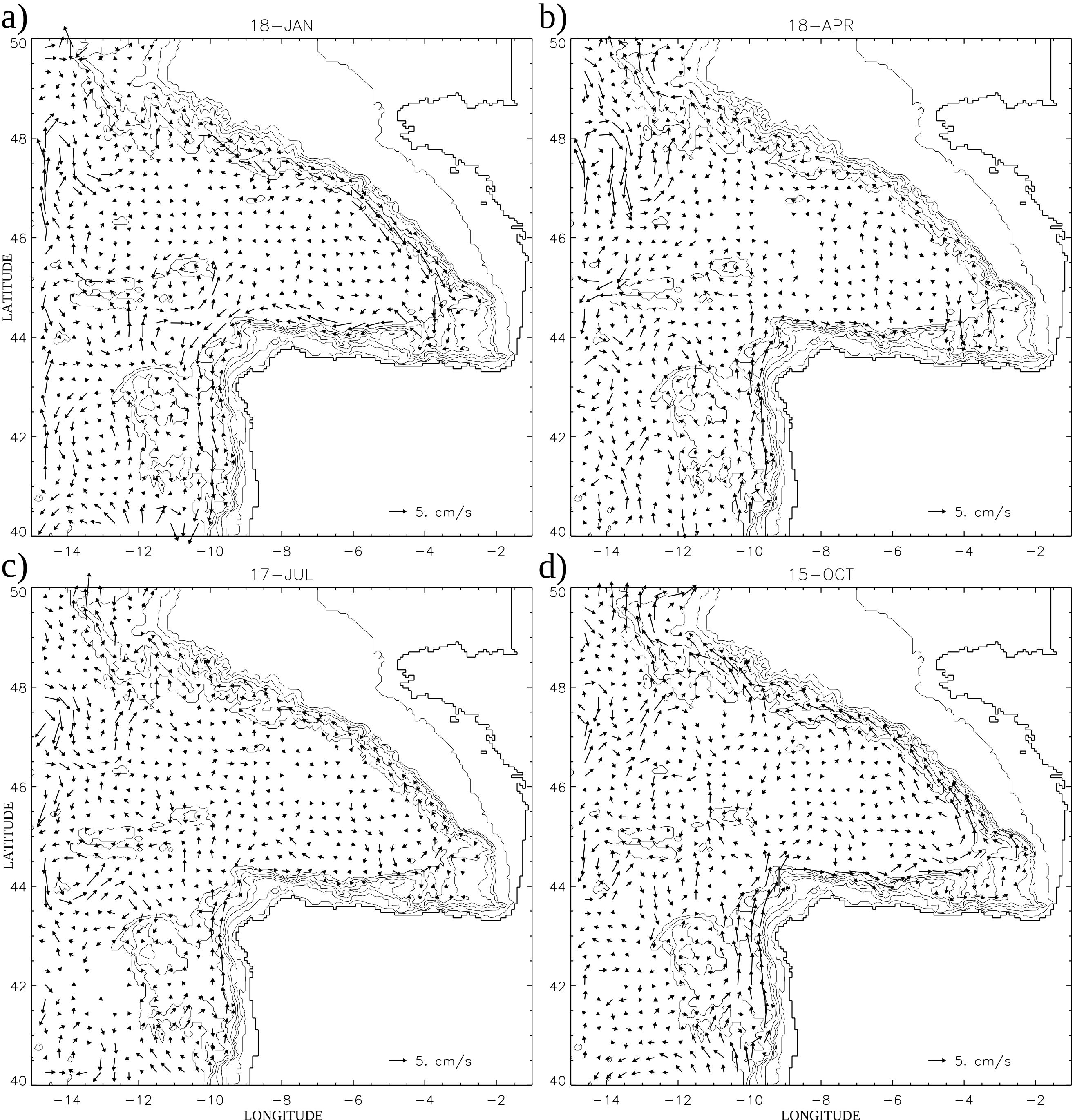

a)
18-JAN
b)
18-APR
c)
17-JUL
d)
15-OCT
LATITUDE
LONGITUDE
5. cm/s
50
48
46
44
42
40
-14
-12
-10
-8
-6
-4
-2

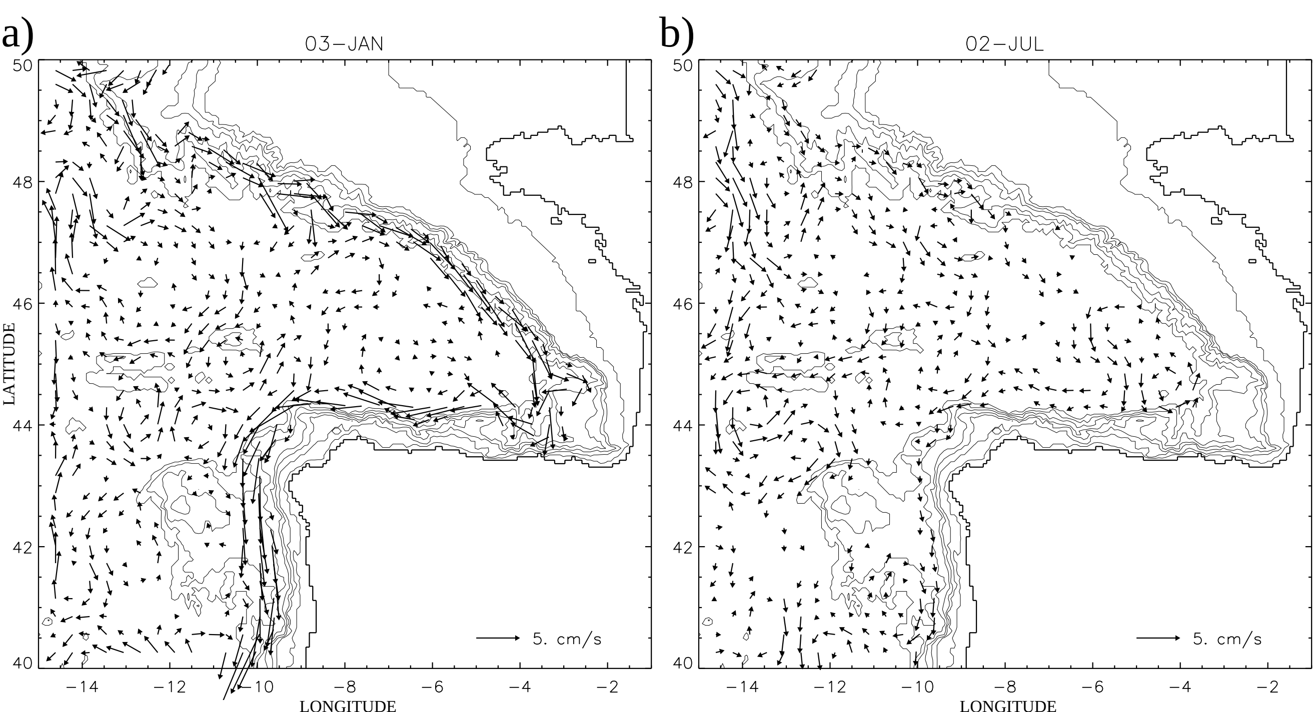
a)
03-JAN
b)
02-JUL
LATITUDE
LONGITUDE
5. cm/s
50
48
46
44
42
40
-14
-12
-10
-8
-6
-4
-2

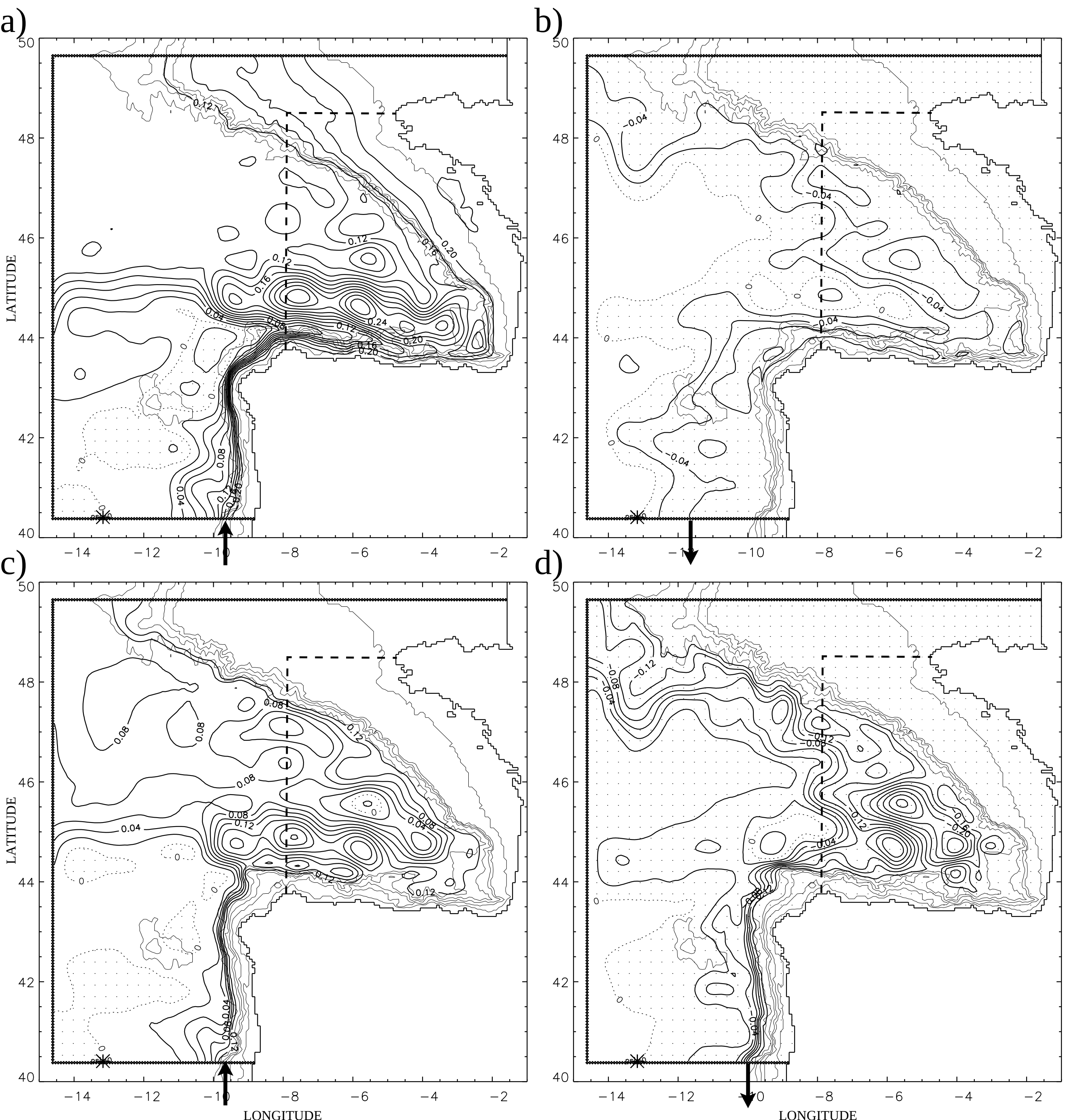
a)
b)
c)
d)
LATITUDE
LONGITUDE
50
48
46
44
42
40
−14
−12
−10
−8
−6
−4
−2